# Quantification of transient signals in multiple collector inductively coupled plasma mass spectrometry: accurate lead isotope ratio determination by laser ablation of individual fluid inclusions†

**Thomas Pettke,‡*[a] Felix Oberli,[a] Andreas Audétat,[b] Uwe Wiechert,§[a] Caroline R. Harris¶[a] and Christoph A. Heinrich[a]**

*Received 1st September 2010, Accepted 31st October 2010*
**DOI: 10.1039/c0ja00140f**



This work establishes the analytical protocol for accurate Pb isotopic analysis of fast transient signals by multiple-collector ICP-MS instruments. Individual synthetic fluid inclusions of known Pb and Tl isotopic compositions (dissolved SRM 981 with or without SRM 997 from NIST, enclosed in quartz by a hydrothermal crack annealing technique) were liberated by 193 nm UV laser ablation (LA). Data were recorded on Faraday detectors, for which correction schemes for bias in amplifier response ("*tau* correction") are presented and evaluated. *tau*-Corrected Pb isotope data reveal LA-induced isotope fractionation amounting to ~0.5% amu$^{-1}$ for Pb isotopes over the course of an entire fluid inclusion ablation. Instrumental mass bias correction was effected within-run using Tl provided by the fluid inclusion itself or admixed to the ablation aerosol *via* desolvated nebulization. Isotope ratios derived from the transient signals were either based on individual readings or on bulk signal integration, of which the latter produces significantly more accurate data. The external precision achieved by ablating SRM 610 glass with a 60 μm beam is ±0.011% (2 SD, relative) for $^{208}$Pb/$^{206}$Pb and $^{207}$Pb/$^{206}$Pb ratios and ±0.032% for Pb isotope ratios normalized to mass 204 ($n = 18$). Inclusion-to-inclusion reproducibilities ($n = 11$; ~0.1 ng Pb per inclusion) are ±0.05% (2 SD; $^{208}$Pb/$^{206}$Pb and $^{207}$Pb/$^{206}$Pb) and ±0.13% ($^{20x}$Pb/$^{204}$Pb), respectively; inclusions containing as little as 0.005 ng Pb returned ±0.1% and ±0.8%. These results are accurate as demonstrated by analysis of synthetic fluid inclusions containing SRM 981 Pb. The analytical protocol presented here for measuring isotope ratios on minute analyte quantities by multiple-collector ICP-MS in fast transient signal mode has great potential for applications to geochemical, archaeological, environmental and possibly biochemical problems.

## Introduction

Laser ablation inductively coupled plasma mass spectrometry (LA-ICP-MS) has demonstrated capabilities in the chemical analysis of solids (*e.g.*, Sylvester[1]) and even heterogeneous inclusions in them, such as fluid or melt inclusions in minerals (*e.g.*, Günther *et al.*,[2] Audétat *et al.*,[3] Halter *et al.*,[4] Heinrich *et al.*,[5] Pettke *et al.*,[6] Allan *et al.*,[7] Spandler *et al.*,[8] Pettke[9]). Latest studies have explored the potential of the LA-ICP-MS technique for *in situ* dating and for the determination of isotope ratios in geochemical, environmental and biological studies. Successful examples of geochemical applications using various isotope systems at adequate precision are rapidly accumulating (*e.g.*, Walder *et al.*,[10] Hirata,[11] Hirata *et al.*,[12] Paul *et al.*,[13] Kosler *et al.*,[14] Jackson and Hart,[15] Paton *et al.*,[16] Gounelle *et al.*,[17] Fietzke *et al.*,[18] Cottle *et al.*,[19] Woodhead *et al.*[20]). Here, we develop the LA-ICP-MS method for using Pb isotopes to trace fluid provenance and migration in ore-forming geological systems.[21]

To obtain accurate and precise isotope ratios by ICP-MS it is crucial to properly correct for mass dependent fractionation and other signal bias occurring at various stages, from the site of laser ablation to that of ion detection. Among possible sources of fractionation, instrumental mass bias is commonly considered to be most prominent. Its nature and possible correction strategies have been investigated in great detail for multiple-collector (MC)-ICP-MS instruments (for the Pb system, see Rehkämper and Mezger,[22] Woodhead,[23] Thirlwall,[24] Albarède *et al.*,[25] Baxter *et al.*[26]). Surprisingly little is known, however, about the nature and extent of isotopic fractionation at the laser ablation site (*e.g.*, Jackson and Günther,[27] Kuhn *et al.*[28]). Thus, the question has remained whether instrumental mass bias at the plasma interface is the dominant, if not the only, factor contributing to the deviation of measured isotope ratios from true values, or whether aerosol generation at the LA site, transport processes and signal recording characteristics may also contribute to the overall bias in isotope ratios encountered.

Instrumental mass bias is dominated by kinetic and space charge effects at the ICP-MS interface. A common correction

[a]*Institute of Geochemistry and Petrology, ETH Zurich, Clausiusstrasse 25, CH-8092 Zurich, Switzerland. E-mail: pettke@geo.unibe.ch*
[b]*Bayerisches Geoinstitut, Universität Bayreuth, D-95440 Bayreuth, Germany*

† Electronic supplementary information (ESI) available: LA-ICP-MS Pb isotope data tables for SRM 610 and SRM 981 Pb synthetic fluid inclusions. See DOI: 10.1039/c0ja00140f

‡ Institute of Geological Sciences, University of Bern, Baltzerstrasse 1 + 3, CH-3012 Bern, Switzerland.
§ Institut für Geologische Wissenschaften, Freie Universität Berlin, D-12249 Berlin, Germany.
¶ Geological and Environmental Sciences, Stanford University, 367 Panama St, Stanford, California 94305, USA.

method requires a pair of non-radiogenic isotopes characterized by an invariant isotopic ratio in nature, ideally from the same element (*e.g.*, Nd, Sr, Hf). This method, originally developed for TIMS isotope analysis, has since successfully been implemented by the ICP-MS community (see reviews by Halliday *et al.*,[29] Albarède *et al.*[25]). Some elements, most importantly Pb, do not possess such an invariant isotope pair, however. At an early stage, Longerich *et al.*[30] therefore proposed to admix Tl, a neighbouring mass element with an invariant isotopic ratio, to the sample and use it for mass bias correction of Pb, assuming that instrumental mass bias is a sole function of mass. As the analytical precision on ICP-MS isotope ratio measurements has improved, notably through the introduction and further development of MC-ICP-MS instruments and double- or triple-spike (enriched isotope) techniques, it became clear that inter-elemental mass bias in ICP-MS instruments is not merely a function of mass (*e.g.*, Rehkämper and Mezger,[22] Thirlwall,[24] Woodhead[23]). Consequently, it was claimed[24,31] that the use of Tl for within-run correction of mass bias would result in Pb isotope data that would be less accurate than those obtained by double- or triple-spike techniques. However, simple modifications to existing mass bias correction protocols using Tl allowed Woodhead[23] to produce MC-ICP-MS Pb isotope data matching double-spike TIMS results in accuracy. An elegant redesign of the mass bias correction protocol by Baxter *et al.*[26] achieves an equivalent level of accuracy for within-run Tl based correction.

In contrast to solution analysis of Pb, where Tl is directly admixed to the sample, the LA-ICP-MS method requires a different approach. Ideally, the sample to be analysed contains naturally occurring, non-fractionated Tl at sufficient concentration to allow for within-run Tl-based instrumental mass bias correction, but this is almost never the case (*e.g.*, Audétat *et al.*[32]). Alternative methods for mass bias correction include (i) admixture of Tl or Pb-spiked aerosol, produced by nebulisation of a Tl standard or Pb spike solution, to the LA aerosol before it enters the ICP, or (ii) bracketing standardization. Matrix matching has been claimed[25] to be vital for highly accurate isotope ratio measurements by bracketing standardization. This approach, widely used for "simple" matrices, is inappropriate for fluid inclusions, because Pb is partly dissolved in the aqueous phase and may partly reside in salt precipitates within the inclusions that are hosted by quartz.

In this study, we document the procedures developed for Pb isotopic analysis of fast transient signals as produced by laser ablation of fluid inclusions in minerals, following a first feasibility test.[33] Our experimental approach is based on fluid inclusion standards prepared with known Pb and Tl isotopic compositions in order to explore different schemes for mass bias correction and possibly discriminate between fractionation occurring at the LA site and in the ICP, respectively. We show that isotope fractionation at the LA site poses no limitation to accuracy provided that fluid inclusion ablation is well controlled. We identify isotope ratio bias related to bias in amplifier response and provide two approaches to correct for these. We explore different signal integration schemes and conclude that the bulk signal integration method provides the most accurate data. Within-run mass bias correction by the methods of both Woodhead[23] and Baxter *et al.*[26] produces accurate Pb isotope data from individual fluid inclusions at precision levels (both within-inclusion and inclusion-to-inclusion), which are only a factor of about five poorer than the best external precision achieved for the NIST SRM 610 standard. An application of our techniques to two assemblages of natural fluid inclusions shows analytical precisions even superior to those obtained on the fluid inclusion standards and thus demonstrates the great potential of this technique for accurate isotope ratio determinations of minute sample amounts recorded in transient signal mode.

## Methods

### Synthetic fluid inclusion standards

Two sets of synthetic fluid inclusion standards were produced, one containing only Pb (SRM 981) and the other prepared with both Pb and Tl (SRM 981 and SRM 997) in an aqueous NaCl–KCl solution of *ca.* 17 wt% bulk salinity (Table 1). A pre-fractured, pure quartz rod (3 × 10 mm) or a stack of etched quartz plates was loaded with $SiO_2$ glass and standard solutions into gold capsules closed by welding. Inclusions were formed at 700 °C/180 MPa over 144 h in cold-seal pressure vessels pressurized with water. Oxygen fugacity was constrained near Ni–NiO by the steel of the pressure vessel and a nickel filler rod. Equal weights of the filled gold capsules before and after the experiment demonstrate that no matter was lost or gained except probably small amounts of hydrogen. Doubly polished thick sections were prepared from the recovered quartz samples. Product inclusions have a bulk density of approximately 0.7–0.8 g $cm^{-3}$ and average sizes of 5–30 μm in diameter, with a few reaching 80 μm. Interestingly, inclusions containing only Pb (Pb-only inclusions) were all rather flat and small while those containing Pb and Tl (Pb–Tl inclusions) formed larger, isometric inclusions (Fig. 1). Repeated runs under varying experimental conditions did not notably improve size and shape of the Pb-only inclusions.

Lead and Tl contents of the synthetic fluid inclusions were determined by LA-ICP-Quadrupole-MS (QMS) at ETH Zurich following methods reviewed by Heinrich *et al.*[5] with instrumental setup and tuning conditions detailed in Pettke *et al.*[6] Resulting concentrations (Table 1) suggest loss of Pb and Tl of up to 20% from the solution *prior* to fluid inclusion formation during the experiment. This could be either due to precipitation of Pb and Tl

**Table 1** Measured Pb and Tl concentrations, and nominal salinity of synthetic fluid inclusion standards

| Sample[a] | NaCl nominal (wt%) | KCl nominal (wt%) | Pb analyzed[b] (μg $g^{-1}$) | Tl analyzed[c] (μg $g^{-1}$) |
|---|---|---|---|---|
| Pb–C1 | 11.7 | 6.2 | 5700 | —[d] |
| Pb–C3 | 11.7 | 6.2 | 5070 | —[d] |
| Pb–C5 | 11.7 | 6.2 | 5480 | —[d] |
| Pb–Tl–A2 | 10.5 | 5.9 | 4030 | 1510 |
| Pb–Tl–A3 | 10.5 | 5.9 | 4430 | 1640 |

[a] No data available for synthesis of Pb–Tl–A4. [b] The nominal Pb concentration in runs Pb–C1 to Pb–C5 was 5500 μg per g of fluid that in Pb–Tl–A2 and Pb–Tl–A3 was 5200 μg $g^{-1}$. [c] The nominal Tl concentration in runs Pb–Tl–A2 and A3 was1790 μg per g of fluid. [d] Absent from synthesis.

 

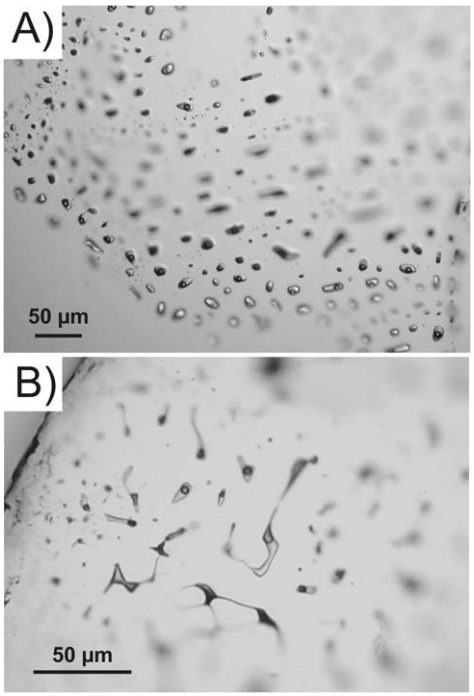


**Fig. 1** Synthetic fluid inclusion standards containing SRM 981 Pb + SRM 997 Tl (A) or SRM 981 Pb only (B) in a Na–K–Cl solution of *ca.* 17 wt% bulk salinity. Note the ellipsoidal to isometric shape of the Pb–Tl fluid inclusions, while the Pb-only fluid inclusions are generally flat, irregular and smaller.

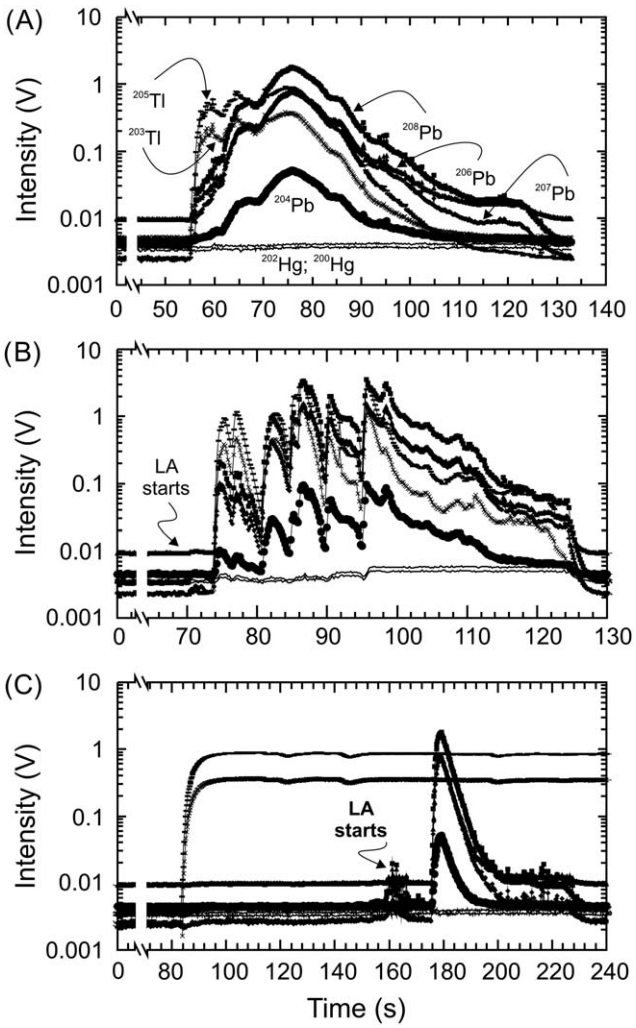


**Fig. 2** Pb and Tl transient isotope signals from fluid inclusion ablation recorded on multiple Faraday detectors. (A and C) Straight ablation (at constant crater size) and (B) step-wise fluid inclusion opening. Signals from large Pb–Tl inclusions (A and B) are characterized by Pb/Tl ratios evolving with progressive inclusion ablation, with signal maxima for Tl shifted towards the start of the ablation. (C) Pb-only inclusion signal produced from inclusion ablation and recorded together with the Tl signal originating from aspirating a SRM 997 Tl solution through a desolvating unit. LA stands for laser ablation.

from the stock solution *prior* to loading (indeed, a few microscopic particles could be observed in the stock solution at the time of capsule loading), or result from loss of Pb and possibly Tl to the Au capsule wall *prior* to inclusion formation. Considering the Pb and Tl concentrations as measured in the synthetic fluid inclusions (Table 1) an egg-shaped Pb–Tl fluid inclusion with longest diameter of 30 µm, the amount of Pb available for analysis is of the order of 0.02 ng. This is considerably less than the amounts consumed for precise MC-ICP-MS isotope analysis of Pb in solution mode using Faraday detectors (isotopic ratios of ±0.01% external precision can be obtained on amounts of Pb as low as *ca.* 5–10 ng[31]). Note that our largest-diameter Pb-only inclusions contain considerably less Pb because of their flatter and more irregular shape and, hence, lower total volume (Fig. 1). Interestingly, Pb–Tl fluid inclusion measurements by both QMS and MC-ICP-MS reveal non-proportional signals for Tl and Pb (*e.g.*, Fig. 2A), indicating that Pb and Tl are not localized in the same inclusion phase at room temperature. Variable bulk fluid inclusion Pb/Tl intensity ratios measured on both MC-ICP-MS and QMS instruments furthermore suggest heterogeneous distribution of Pb and Tl in the product inclusions.

## LA-MC-ICP-MS instrument details and analytical strategies

All LA-MC-ICP-MS Pb isotope analyses were performed at ETH Zurich using a GeoLas 200Q (Lambda Physik, Germany) laser system with computer-controlled sample stage connected to either a Nu Plasma or a Nu Plasma 1700 MC-ICP-MS instrument (Nu Instruments Ltd, Wrexham, UK). Table 2 summarizes the operating conditions for LA-ICP-MS analysis of Pb isotopes, plus the ranges in parameters explored during this study. An energy-homogenized laser beam profile with sufficient energy density on the sample surface (>15 J $cm^{-2}$) is essential for controlled ablation of fluid inclusions in quartz.[5] The first feasibility tests using a MC-ICP-MS instrument[33] achieved analytical precisions for individual inclusions considerably better than those reported for sequential signal recording using a quadrupole instrument. The latter technique is hampered by limitations in representative recording of fast transient signals[34] and poor duty cycle, whereas for simultaneous ion detection the duty cycle is nearly an order of magnitude larger for the isotope sequence analysed here (Table 2). Therefore, single-collector instruments were not further evaluated in this study.

**Table 2** LA-ICP-MS instrument and data acquisition parameters

| | |
|---|---|
| Compex 110I Excimer 193 nm ArF laser[a] | |
| Energy density on sample/J cm$^{-2}$ | *ca.* 16 (10–25), homogeneous energy distribution across the ablation crater |
| Pulse duration/ns | *ca.* 15 |
| Repetition rate/Hz | SRM:[b] 6 (1–10), FI:[c] 10 |
| Shooting mode | 1 μm s$^{-1}$ line scan (SRM), single spot (SRM, FI) |
| Crater sizes/μm | SRM: 60, variable for FI (8–80) |
| Ablation cell volume/cm$^3$ | FI: 1, variable for SRM (1–16) |
| Helium cell gas flow/l min$^{-1}$ | 0.5–0.8 (0.3–1.3) |
| Nu Plasma MC-ICP-MS[a] | |
| Desolvating nebulizer unit | MCN-6000 |
| Process gas | Ar |
| Power/W | 1400 (1100–1500) fwd; <2 refl. |
| Accelerating voltage/kV | 4 |
| Detector mode | Multiple Faradays |
| Mass resolution | *ca.* 400 (10% valley) |
| Nu Plasma 1700 MC-ICP-MS[a] | |
| Desolvating nebulizer unit | DSN-100 (Nu Instruments Ltd) |
| Process gas | Ar |
| Power/W | 1450 (1100–1550) fwd; <2 refl. |
| Accelerating voltage/kV | 6 |
| Detector mode | Multiple Faradays |
| Mass resolution per amu | *ca.* 700 (10% valley) |
| Data acquisition parameters during transient signal analysis, both instruments[a] | |
| Acquisition mode | Static |
| Integration time | 200 ms per reading |
| Baseline measurement | On peak with laser beam off |
| Masses analyzed | 200, 202, 203, 204, 205, 206, 207, 208 |

[a] Values reported in brackets are the ranges explored. [b] SRM refers to SRM 610 glass from NIST. [c] FI refers to fluid inclusions.

Before the helium stream transporting the aerosol from the LA chamber enters the torch, an Ar-based aerosol is admixed from a desolvator aspirating an ultrapure ~1% $HNO_3$ solution containing either Tl or no metal. The MC-ICP-MS instruments were optimized daily for maximum sensitivity, perfect peak flatness and coincidence by admixing a desolvated aerosol generated from a 30 ng g$^{-1}$ Pb–32 ng g$^{-1}$ Tl solution to the He flow from the LA chamber. Minor re-tuning was then performed using an aerosol produced from SRM 610 laser ablation in line scan mode (Table 2), while aspirating a pure 1% $HNO_3$ solution. Optimization with Ar alone (*i.e.*, without a He flow from the LA chamber) is inadequate because the focusing properties of the MC-ICP-MS instruments are rather sensitive to gas composition and flow rate.

The analyses were performed in static time-resolved mode using a modified instrument control and data acquisition software, collecting $^{200}$Hg–$^{202}$Hg–$^{203}$Tl–$^{204}$(Hg, Pb)–$^{205}$Tl–$^{206}$Pb–$^{207}$Pb–$^{208}$Pb simultaneously in 8 Faraday cups calibrated daily for their preamplifier gains. All experiments were performed with the same Tl standard solution. However, care was taken not to expose the solution to light during storage in order to avoid variations in Tl speciation potentially leading to mass fractionation effects during the desolvating process.[35] The signals at masses 200–208 were recorded at 0.2 s integration intervals. For the measurement of samples containing both Pb and Tl (SRM 610 glass and Pb–Tl inclusions), the LA signal was acquired after having collected the background on peak for at least 50 seconds (laser pulsing turned off), while aspirating a pure 1% $HNO_3$ solution (Fig. 2A and B). For Pb-only inclusions, the background was acquired in the same way, then the Tl-solution was aspirated, and once the Tl signal was stable, LA was started, superimposing the fluid inclusion signal on the Tl signal from the desolvating unit (Fig. 2C). Sections for background and signal processing were carefully chosen by re-evaluation of each measurement off-line using criteria detailed below. Mass bias correction was exclusively done in within-run mode. Optimum Pb sensitivities determined on desolvated Pb–Tl standard solutions in this mixed Ar–He plasma mode were about 250 V (Nu Plasma 1700) and 180 V (Nu Plasma) relative to a Pb concentration of 1 μg per g of solution, at uptake rates of approx. 80 μl per minute.

LA conditions and interface setup were optimized by a series of tests at different experimental conditions using SRM 610 glass. The final parameters derived from these experiments (Table 2) were then applied to fluid inclusion analysis. Each set of fluid inclusion analyses was bracketed by 2–3 measurements on SRM 610 glass in order to monitor machine performance. Mass bias relationships between Pb and Tl were established based on the total set of SRM 610 measurements acquired over the duration of the project and then applied to the individual fluid inclusion analyses based on measured Tl aspirated through a desolvating unit or contained by the inclusions. The SRM 610 standard measurements were always done in line-scan mode (1 μm s$^{-1}$ transport rate, 60 μm spot size, 6 Hz pulse repetition rate, 90 s signal recording), after having ensured that single-spot and line-scan mode give the same Pb isotopic results at >2 Hz laser repetition rate.

## Data reduction

Transient signal data reduction was done by revisiting the individually stored readings using the modified Nu Instruments software (steps 1–4), followed by off-line evaluation on Excel spreadsheets (step 5). (1) Individual raw readings were corrected for amplifier response effects (referred to as *tau* correction and outlined in detail below), since the original instrument software does not provide for appropriate correction of fast transient signals. (2) The readings from selected background sections were averaged and used for baseline correction of individual, simultaneously acquired 0.2 s readings from selected signal sections, followed by (3) an interference correction for Hg contribution to mass 204 based on $^{202}$Hg. (4) Two different approaches to derive mean isotopic ratios for an individual fluid inclusion were explored in our study. In a first approach named the "individual reading integration method", isotopic ratios were calculated for individual background- and interference-corrected 0.2 s signal readings, filtered by a one-pass 2σ outlier removal test, then averaged and finally (5) corrected off-line for mass bias (all data reported in Tables S1 and S2† have been reduced this way). In a second approach named "bulk signal integration method", the background-corrected signal intensities were summed up, and further data reduction then carried out on this single set of integrated intensity readings.

The Hg interference correction on mass 204 in step 3 was based on the measured $^{202}$Hg beam and a $^{202}$Hg/$^{204}$Hg ratio of 4.32, adjusted to the fractionated state by use of an exponential mass bias coefficient derived from the measured $^{205}$Tl/$^{203}$Tl ratio and its common value of 2.3871.[36] Final mass-bias corrected $^{20x}$Pb/$^{204}$Pb

 

ratios do not correlate with $^{202}Hg/Pb_{(total)}$, demonstrating successful removal of Hg interference. Owing to low beam intensities on Faraday cups, the measured $^{202}Hg/^{200}Hg$ isotope ratio could not be measured precisely enough to directly derive a fractionation coefficient for Hg. The Hg intensity of the gas background, too, was insufficient for determining a precise Hg-specific mass bias (*cf.* Paul *et al.*[13]). As will be shown below, correction for $^{204}Hg$ interference alone based on $^{202}Hg$ produces sufficiently accurate results and thus demonstrates that other potential interferences (*e.g.*, $WO^+$, REE argides) are not relevant at the level of our external analytical precision.

Mass bias correction in step 5 was effected using the refined empirical procedure of Baxter *et al.*[26] for obtaining mass-bias corrected isotope ratios with minimized uncertainty magnification. This procedure establishes *lnTl–lnPb* relationships that are machine- and isotope ratio specific. It uses the linear relationship in *ln–ln* space between the mass biases of the internal standard (Tl) and the target (Pb) isotope ratios measured in the sample (*i.e.*, the fluid inclusions) and relates it to that established experimentally on the reference material (SRM 610 glass here). All robust SRM 610 data acquired during several years since setting up the LA-ICP-MS fluid inclusion analytical method were used to define such *lnTl–lnPb* relationships. These long-term, well-defined average fractionation trends were then employed for mass bias correction because the spread in *lnTl–lnPb* values from individual analytical sessions was always too small to derive well-defined linear regression parameters. During the development of methods, significant modifications of the ICP-MS front end such as the use of different types of sampler and skimmer cones and reduction of interface pressure to the values reported in Table 2 were implemented. This caused a considerable range in instrumental mass bias, thus enhancing the definition of the *lnTl–lnPb* relationships. Individual fluid inclusion analyses were thus corrected for mass bias using the within-run measured $^{205}Tl/^{203}Tl$ isotope ratio and the Baxter *et al.*[26] approach, after ensuring that the bracketing SRM 610 measurements were consistent with our long-term *lnTl–lnPb* relationships. Previously, Woodhead[23] derived a $f_{Tl}$–$f_{Pb}$ relationship, the use of which returned identical results (within uncertainties) for our dataset. Resulting fluid inclusion Pb isotope ratios are accurate at the external precisions achieved by the LA-MC-ICP-MS analyses (see below).

## Results and discussion

### SRM 610 data

All datasets obtained on the SRM 610 standard glass and used for establishing the mass-bias correction parameters are listed in Table S1 (ESI†). The data include homogeneity tests on SRM 610, variations in laser pulse repetition rate and laser energy for single spot ablation and scanning experiments as well as results on standard runs interspersed with the fluid inclusion analyses. Acquired during several years, these data display remarkably correlated trends with few outliers. Outliers in $f_{^{208}Pb/^{206}Pb}$ and $f_{^{207}Pb/^{206}Pb}$ *vs.* $f_{Tl}$ plots (not shown) are analyses with Pb/Tl intensity ratios as high as 34, well above Pb/Tl = 6 to 8 as commonly measured. These elevated Pb/Tl ratios identify zones in the SRM 610 glass characterized by variably enhanced loss of Tl during glass manufacture (*e.g.*, Eggins and Shelley;[37] Kent[38]), which also may have caused isotopic fractionation. Therefore, SRM 610 analyses with Pb/Tl intensity ratios >9 were discarded. This is a robust criterion, since day-to-day variability in Pb/Tl intensity ratios that could result from differences in the daily tuning of the LA-ICP-MS instrument was only marginally larger than within-day variability.

The large SRM 610 dataset collected for this study allows evaluation of analytical precision at various scales, from internal (within-run) precision to that achieved during the entire development of methods (Table S1†). Analytical accuracy, on the other hand, cannot be evaluated from this dataset as it serves as a base for the calibration of the unknown Pb isotope composition of the fluid inclusions. The external reproducibility of the mass-bias corrected isotope ratios achieved within one analytical session on Nu Plasma 1700 was *ca.* 110 ppm (2 SD, $n = 18$) for $^{208}Pb/^{206}Pb$ and $^{207}Pb/^{206}Pb$ ratios, and 320 ppm for Pb isotope ratios relative to mass 204 (Table 3), the long-term external reproducibility being only slightly larger. The same uncertainties expressed as two standard errors of the mean of the 18 analyses of that session are 26 and 75 ppm, respectively. Our analytical reproducibility compares well with LA-MC-ICP-MS data reported elsewhere[39] for SRM 610 (see also Paul *et al.*[13]). The measurement session at Nu Plasma 1700 referred to (data from August 30, 2005; Table 3) included 3 ablation chamber loadings and lasted for about 13 hours. The amount of Pb consumed per line scan analysis is *ca.* 300–400 pg. The reduced precision on mass 204 is due to low beam intensities of 3.5–5.0 $\times 10^{-13}$ A, resulting in some correlation in $^{20x}Pb/^{204}Pb$ *vs.* $^{20y}Pb/^{204}Pb$ plots (Fig. 3A). This correlation cannot be due to inadequate mass bias correction, since other combinations of mass bias corrected isotope ratios (*e.g.*, $^{207}Pb/^{204}Pb$ *vs.* $^{208}Pb/^{206}Pb$, Fig. 3B) do not show such correlation and because the slope of the data array is indicative of error predominantly associated with the measurement of mass 204. Data obtained on Nu Plasma exhibit the same overall features but external precision is somewhat poorer (Table 3), partially owing to the lower sensitivity achieved for laser ablation using this instrument.

Woodhead[23] made use of matrix effects (variation in chemical purity of the analyte) to create sufficient spread in $f_{Tl}$–$f_{Pb}$ to precisely define their functional relationship, but the invariant matrix of our reference material (SRM 610) did not allow for such an approach. Instead, we had to rely on variations of our interface configuration (*e.g.*, choice of cones and interface pressures) and operating conditions such as ablation chamber (He) and desolvator (Ar) gas flows during the course of this study. The observed variations in our $f_{Tl}$ and $f_{Pb}$ values are thus predominantly related to variations in the ion production and extraction processes, which are also influenced by daily ICP-MS optimization. It is remarkable indeed that for each instrument and Pb isotope ratio, a systematic $f_{Tl}$–$f_{Pb}$ relationship can be maintained over several years in spite of substantial hardware modifications.

The effect of peak tailing interference on mass 204 from a large $^{205}Tl$ peak (*e.g.*, Thirlwall[24]) as could be obtained when admixing Tl *via* desolvated nebulisation during sample measurement is calculated to be insignificant in our case for measured Pb/Tl intensity ratios of 1 or higher, at the external reproducibility achieved in LA-ICP-MS mode. The abundance sensitivities are approximately 1–2 $\times 10^{-6}$ for the Nu Plasma 1700 and ~2 to 4 $\times 10^{-6}$ for the Nu Plasma instruments at mass 237.

**Table 3** Selected LA-ICP-MS data for SRM 610 glass bracketing fluid inclusion analyses[a]

| Run | $^{208}Pb/^{206}Pb$ | 1 SE abs. | $^{207}Pb/^{206}Pb$ | 1 SE abs. | $^{206}Pb/^{204}Pb$ | 1 SE abs. | $^{207}Pb/^{204}Pb$ | 1 SE abs. | $^{208}Pb/^{204}Pb$ | 1 SE abs. |
|---|---|---|---|---|---|---|---|---|---|---|
| NU Plasma 1700: August 30 | | | | | | | | | | |
| SRM610_Aug30-05_1 | 2.16932 | 0.00015 | 0.90988 | 0.00004 | 17.0502 | 0.0017 | 15.5136 | 0.0018 | 36.9836 | 0.0050 |
| SRM610_Aug30-05_2 | 2.16919 | 0.00014 | 0.90987 | 0.00004 | 17.0505 | 0.0018 | 15.5139 | 0.0019 | 36.9851 | 0.0052 |
| SRM610_Aug30-05_3 | 2.16908 | 0.00016 | 0.90978 | 0.00004 | 17.0484 | 0.0020 | 15.5098 | 0.0022 | 36.9782 | 0.0060 |
| SRM610_Aug30-05_4 | 2.16910 | 0.00015 | 0.90978 | 0.00004 | 17.0457 | 0.0017 | 15.5071 | 0.0018 | 36.9697 | 0.0052 |
| SRM610_Aug30-05_5 | 2.16920 | 0.00014 | 0.90977 | 0.00004 | 17.0515 | 0.0018 | 15.5117 | 0.0019 | 36.9853 | 0.0053 |
| SRM610_Aug30-05_6 | 2.16912 | 0.00015 | 0.90976 | 0.00004 | 17.0484 | 0.0017 | 15.5105 | 0.0019 | 36.9789 | 0.0053 |
| SRM610_Aug30-05_7 | 2.16935 | 0.00013 | 0.90986 | 0.00003 | 17.0522 | 0.0018 | 15.5142 | 0.0017 | 36.9889 | 0.0046 |
| SRM610_Aug30-05_8 | 2.16905 | 0.00014 | 0.90982 | 0.00004 | 17.0492 | 0.0018 | 15.5109 | 0.0019 | 36.9776 | 0.0052 |
| SRM610_Aug30-05_9 | 2.16923 | 0.00013 | 0.90980 | 0.00003 | 17.0474 | 0.0016 | 15.5096 | 0.0017 | 36.9778 | 0.0045 |
| SRM610_Aug30-05_10 | 2.16921 | 0.00016 | 0.90982 | 0.00004 | 17.0461 | 0.0021 | 15.5088 | 0.0021 | 36.9715 | 0.0058 |
| SRM610_Aug30-05_11 | 2.16933 | 0.00015 | 0.90989 | 0.00004 | 17.0483 | 0.0021 | 15.5118 | 0.0021 | 36.9799 | 0.0058 |
| SRM610_Aug30-05_12 | 2.16924 | 0.00015 | 0.90982 | 0.00004 | 17.0488 | 0.0020 | 15.5109 | 0.0019 | 36.9779 | 0.0052 |
| SRM610_Aug30-05_13 | 2.16922 | 0.00013 | 0.90983 | 0.00003 | 17.0456 | 0.0017 | 15.5082 | 0.0017 | 36.9720 | 0.0047 |
| SRM610_Aug30-05_14 | 2.16937 | 0.00014 | 0.90991 | 0.00004 | 17.0463 | 0.0017 | 15.5100 | 0.0017 | 36.9743 | 0.0046 |
| SRM610_Aug30-05_15 | 2.16928 | 0.00013 | 0.90987 | 0.00003 | 17.0471 | 0.0017 | 15.5106 | 0.0017 | 36.9759 | 0.0048 |
| SRM610_Aug30-05_16 | 2.16953 | 0.00012 | 0.90992 | 0.00003 | 17.0449 | 0.0017 | 15.5107 | 0.0018 | 36.9790 | 0.0048 |
| SRM610_Aug30-05_17 | 2.16910 | 0.00013 | 0.90980 | 0.00004 | 17.0443 | 0.0018 | 15.5065 | 0.0019 | 36.9655 | 0.0051 |
| SRM610_Aug30-05_18 | 2.16942 | 0.00012 | 0.90984 | 0.00003 | 17.0415 | 0.0019 | 15.5056 | 0.0019 | 36.9692 | 0.0051 |
| **Daily average** | 2.16924 | | 0.90984 | | 17.0476 | | 15.5102 | | 36.9772 | |
| 2 SD (absolute) | 0.00026 | | 0.00010 | | 0.0054 | | 0.0048 | | 0.0123 | |
| 2 SD (ppm) | 119 | | 105 | | 318 | | 310 | | 334 | |
| 2 SE (absolute) | 0.00006 | | 0.00002 | | 0.00128 | | 0.00113 | | 0.00291 | |
| 2 SE (ppm) | 28 | | 25 | | 75 | | 73 | | 79 | |
| NU Plasma: August 23 | | | | | | | | | | |
| SRM610_1 | 2.16988 | 0.00017 | 0.90996 | 0.00004 | 17.0562 | 0.0035 | 15.5186 | 0.0031 | 37.0057 | 0.0073 |
| SRM610_2 | 2.17000 | 0.00022 | 0.91003 | 0.00006 | 17.0620 | 0.0041 | 15.5270 | 0.0037 | 37.0223 | 0.0088 |
| SRM610_20 | 2.17007 | 0.00021 | 0.91001 | 0.00005 | 17.0628 | 0.0050 | 15.5266 | 0.0047 | 37.0230 | 0.0110 |
| SRM610_21 | 2.16976 | 0.00015 | 0.90995 | 0.00004 | 17.0475 | 0.0030 | 15.5131 | 0.0028 | 36.9884 | 0.0070 |
| SRM610_22 | 2.16981 | 0.00015 | 0.90994 | 0.00004 | 17.0437 | 0.0031 | 15.5098 | 0.0028 | 36.9846 | 0.0070 |
| SRM610_23 | 2.16991 | 0.00014 | 0.90996 | 0.00004 | 17.0417 | 0.0027 | 15.5092 | 0.0026 | 36.9792 | 0.0066 |
| SRM610_24 | 2.16952 | 0.00015 | 0.90992 | 0.00004 | 17.0524 | 0.0029 | 15.5173 | 0.0027 | 36.9948 | 0.0068 |
| SRM610_30 | 2.16997 | 0.00015 | 0.90998 | 0.00004 | 17.0451 | 0.0031 | 15.5126 | 0.0030 | 36.9867 | 0.0074 |
| SRM610_31 | 2.17003 | 0.00015 | 0.91003 | 0.00004 | 17.0450 | 0.0031 | 15.5112 | 0.0029 | 36.9868 | 0.0071 |
| SRM610_32 | 2.17014 | 0.00014 | 0.91008 | 0.00004 | 17.0482 | 0.0028 | 15.5153 | 0.0026 | 36.9961 | 0.0065 |
| SRM610_33 | 2.16976 | 0.00015 | 0.90996 | 0.00005 | 17.0463 | 0.0032 | 15.5125 | 0.0029 | 36.9869 | 0.0072 |
| **Daily average** | 2.16990 | | 0.90998 | | 17.0501 | | 15.5157 | | 36.9959 | |
| 2 SD (absolute) | 0.00035 | | 0.00009 | | 0.0146 | | 0.0124 | | 0.0299 | |
| 2 SD (ppm) | 162 | | 104 | | 856 | | 797 | | 809 | |
| 2 SE (absolute) | 0.00011 | | 0.00003 | | 0.0044 | | 0.0037 | | 0.0090 | |
| 2 SE (ppm) | 49 | | 31 | | 258 | | 240 | | 244 | |

[a] All shots were acquired in line scan mode (1 μm $s^{-1}$ transport rate, 6Hz, 60 μm spot size). Uncertainties given for individual fluid inclusions are 1 standard error of measurement.

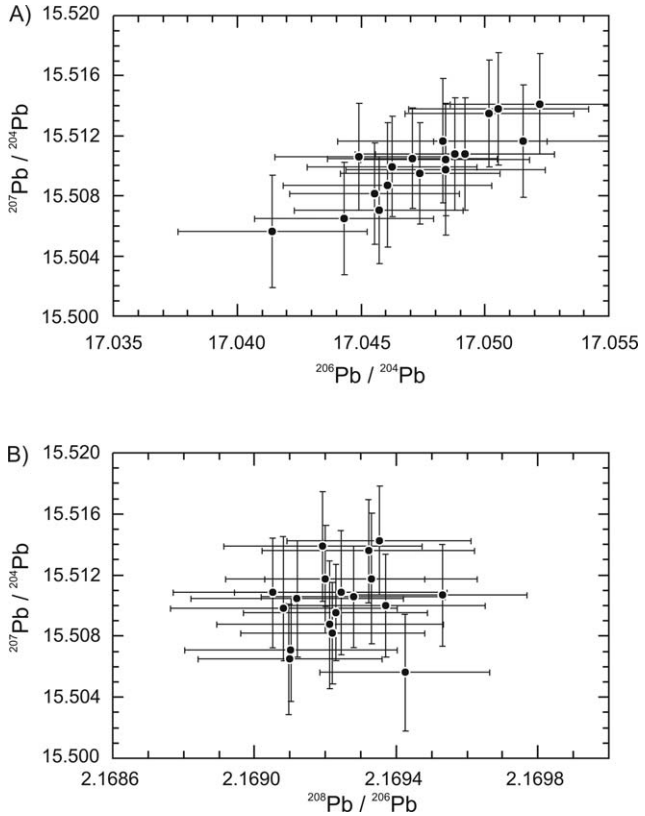


**Fig. 3** (A) $^{207}$Pb/$^{204}$Pb *vs.* $^{208}$Pb/$^{206}$Pb laser ablation data of SRM 610 glass show that correction for mass-dependent isotope fractionation (mass bias) following Baxter *et al.*[26] leaves no residual correlation. (B) A plot of isotope ratios with mass 204 in the denominator reveals a linear trend, indicative of correlation due to elevated uncertainty for mass 204. Error bars are 2 SE measurement uncertainties.

### Synthetic fluid inclusions

Data acquired during method testing reveal that it is important to control the ablation process of inclusions, in such a way that smooth signals conducive to accurate data integration are produced, rather than short signal spikes caused by "explosion" of the inclusion or breakage of the host quartz. The ablation process was therefore routinely monitored on a video screen. The best analyses were achieved for inclusions of up to *ca.* 50 μm largest diameter located 50–80 μm below sample surface, by enlarging the diameter of the pit in step-wise fashion to the final pit size *before* the inclusion was intersected (Fig. 2C, *straight ablation technique*[9]). A step-wise enlargement of the pit *during* inclusion ablation (*step-wise opening technique*,[2] Fig. 2B) was not beneficial because the overall signal-to-noise ratio decreases when the same total amount of ions available from the inclusion is analyzed over a longer period and because of very rapid changes in signal intensity (see below). This holds in particular for mass 204, where an unduly slow ablation process can yield uncertainties which render the data useless.

### Isotope ratio evolution trends during an individual inclusion analysis

Inspection of the time-resolved, background-corrected analyte intensities measured at 0.2 s reading intervals reveals that isotope ratios evolve with progressive ablation of an individual fluid inclusion. For Pb–Tl inclusions, where Pb and Tl are both provided by the fluid inclusions, both Pb and Tl show evolving isotope ratios (Fig. 4A and B), spanning several percent, whereas $^{205}$Tl/$^{203}$Tl does not evolve across the fluid inclusion ablation when Tl is admixed through desolvating nebulisation as for Pb-only inclusions (Fig. 4C and D). In detail, raw $^{208}$Pb/$^{206}$Pb ratios become lighter while $^{205}$Tl/$^{203}$Tl ratios become heavier with progressive ablation, inconsistent with simple laser-ablation induced mass-dependent fractionation. One or more other dominant ratio biasing processes are thus indicated.

Instrumental mass bias at the plasma-interface region cannot explain the effect. The constancy of the measured $^{205}$Tl/$^{203}$Tl ratio displayed in Fig. 4D demonstrates that the concurrently variable Pb isotope ratios (Fig. 4C) are not due to fluctuations in mass bias at this region such as could be caused by variations in matrix composition during fluid inclusion ablation. Such matrix variations are likely to be subtle in any case, because the bulk aerosol load in the plasma is dominated by host quartz contribution, as the beam size is chosen to exceed the largest diameter of the fluid inclusion in order to ensure complete ablation.[2,9]

The observed isotope ratio trends thus appear to be closely linked to problems associated with the recording of transient signals characterized by rapidly changing intensities. Evolving isotope ratios for transient analyte signals have been reported for thermal desorption of Hg from gold traps[40] and for analytes supplied by gas chromatography[41,42] or liquid chromatography.[43] Whereas such observations, at least in part, are likely to relate to real mass fractionation effects accompanying the pre-processing of the analyte *prior* to its introduction to the plasma, bias can also be expected from the recording electronics of the instrument such as caused by differences in amplifier response among the Faraday collectors employed for multi-collector measurements. A quantitative treatment of this problem is presented in the following section.

### Amplifier response bias: numerical correction schemes

Several studies involving transient signal processing have shown that isotopic ratios derived from rapidly rising or decreasing signals can be affected by amplifier response.[12,19,43] Such variations are also displayed by the $^{208}$Pb/$^{206}$Pb isotope ratios of two fluid inclusions analyzed by the straight ablation technique (Fig. 5A) and by the stepwise opening procedure (Fig. 5D), respectively. Variations in $^{208}$Pb/$^{206}$Pb correlate with the intensity variation between sequential 0.2 s readings, which is particularly evident in the stepwise opened fluid inclusion (Fig. 5D). Variations in isotopic ratio during a static multiple collector measurement are therefore expected from any differences in the settling parameters of the Faraday amplifiers used in the analysis. Uncorrected, the amplifier outputs will lag behind the input (ion) signal after a change of beam intensity, and depending on which amplifiers are faster or slower, signals become enhanced or reduced relative to each other. Ratio bias is thus a function of input signal gradient and opposite for positive and negative gradients (Fig. 5D, see also Fig. 1 in Hirata *et al.*[12]).

Here, we present two approaches to correct for this problem, which we will call (1) the stepping *tau* correction and (2) the

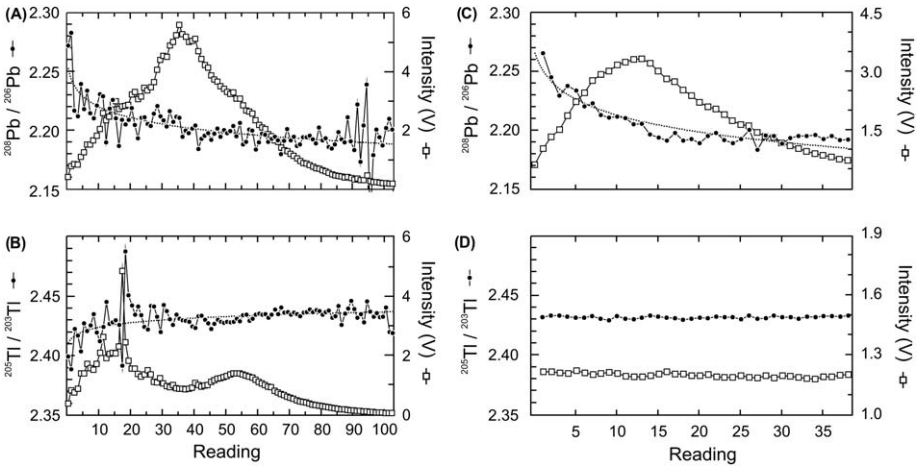


**Fig. 4** Plot of background-corrected Pb (A and C) and Tl (B and D) isotope ratios (filled circles) calculated for individual 0.2 s integration intervals (readings), and corresponding total Pb and Tl signal intensities (open squares). The sections shown cover the entire signal interval integrated for two fluid inclusion analyses. Both fluid inclusions were liberated by the straight ablation technique. All the isotope ratios are plotted at the same scale. Trend lines (dotted) are shown in (A), (B) and (C). Raw Pb isotopic ratios evolve for both Pb–Tl inclusions (A) and Pb-only inclusions (C). For Pb–Tl inclusions, the measured $^{205}Tl/^{203}Tl$ ratio (all Tl supplied by the inclusion) also evolves with progressive ablation of the inclusion (B), while it remains constant for the Pb-only inclusions (D), where Tl is supplied from desolvated aerosol. Note the larger scatter of isotope ratios at the beginning and end of the transient signal trace (A and B), resulting from reduced analytical precision at the low-intensity tails. The evolution of the background-corrected Pb isotopic ratios during progressive fluid inclusion ablation is mainly due to differences in response of the Faraday amplifiers used for recording the masses (see Fig. 5 and text for explanations).

quadratic *tau* correction. In essence, signal decay functions are empirically determined for each Faraday detector and then applied to remove residual bias resulting from *prior* signal variations from the individual readings. To this aim, the existing instrument software of Nu Plasma 1700 was modified and expanded to allow for calibration of settling parameters required for each of the 16 Faraday amplifiers of the instrument. A typical calibration procedure consisted of repeat exposures of the Faraday collector to ion beams of $\sim 8 \times 10^{-11}$ A (using $10^{11}$ Ω feedback resistors) for 60 s, each followed by a measurement of the signal decay curve *vs.* time for another 60 s after beam cut-off. The timing chosen for such an experiment depends on the decay characteristics of the particular system to be calibrated. For adequate processing of fast transient signals, proper calibration of the decay segment extending over fractions of seconds to a few seconds immediately following beam cut-off is of great importance. This requires a fast mechanism for cutting the beam. Rather than relying on the standard method of applying a voltage offset to the electrostatic analyzer (ESA) for beam deflection, we use a pair of vertical deflectors located at the exit region of the ESA, which allows for faster beam control. The measurement of beam intensity and signal decay is performed at 0.1 s integration, the fastest reading rate available for the digital voltmeters (DVMs) used. Each DVM reading is associated with a time stamp read from the high-resolution performance counter of the computer controlling the instrument. A series of such measurements was bracketed between two baseline measurements of 60 s each, preceded by waiting intervals of 180 s at beam-off conditions allowing the collector system to fully discharge. In order to derive amplifier response parameters, which then can be applied to correct the measurements, we model the decay curve as a sum of discrete RC decay terms

$$\mathrm{res}(t) = \sum_{j=1}^{n} a_j \mathrm{e}^{-t/\tau_j} \quad (1)$$

where res($t$) denotes the baseline-corrected residual signal intensity $t$ seconds after beam cut-off divided by the baseline-corrected beam intensity, $a_j$ is a pre-exponential coefficient, $\tau_j = R_j C_j$ the time constant for the $j^{\mathrm{th}}$ term, and $n$ is the number of summation terms required to adequately reproduce the decay curve. $\sum_{j=1}^{n} a_j = 1$, such that res(0) = 1, equivalent to the full signal at the time of beam cut-off.

For proper application of this model to the real experiment, one needs to consider that the signal readings are based on integration over intervals of time rather than point measurements in time. To describe the decay curve as observed by integrated readings, eqn (1) is rewritten as

$$\mathrm{resInt}(t) = \sum_{j=1}^{n} \frac{a_j \tau_j}{\Delta t}\left(\mathrm{e}^{-t/\tau_j} - \mathrm{e}^{-(t+\Delta t)/\tau_j}\right) \quad (2)$$

where resInt($t$) is the residual signal as seen by integration over the time interval from $t$ to $t + \Delta t$, $t$ being the time elapsed since beam cut-off. From the repeat decay experiments, mean values and their errors are calculated for the signals and their time stamps, to serve as input data for the determination of the decay parameters $a_j$ and $\tau_j$ by error weighted least-squares regression on eqn (2). For the Faraday amplifiers of our instrument, $n \geq 4$ typically provides for adequate fitting of the decay curves over their recorded lengths.

A simple application of these parameters for correction of the measurements is to treat the intensity variation between subsequent readings as a step response function such that eqn (2) can be applied to this task. For a series of readings sequentially

 

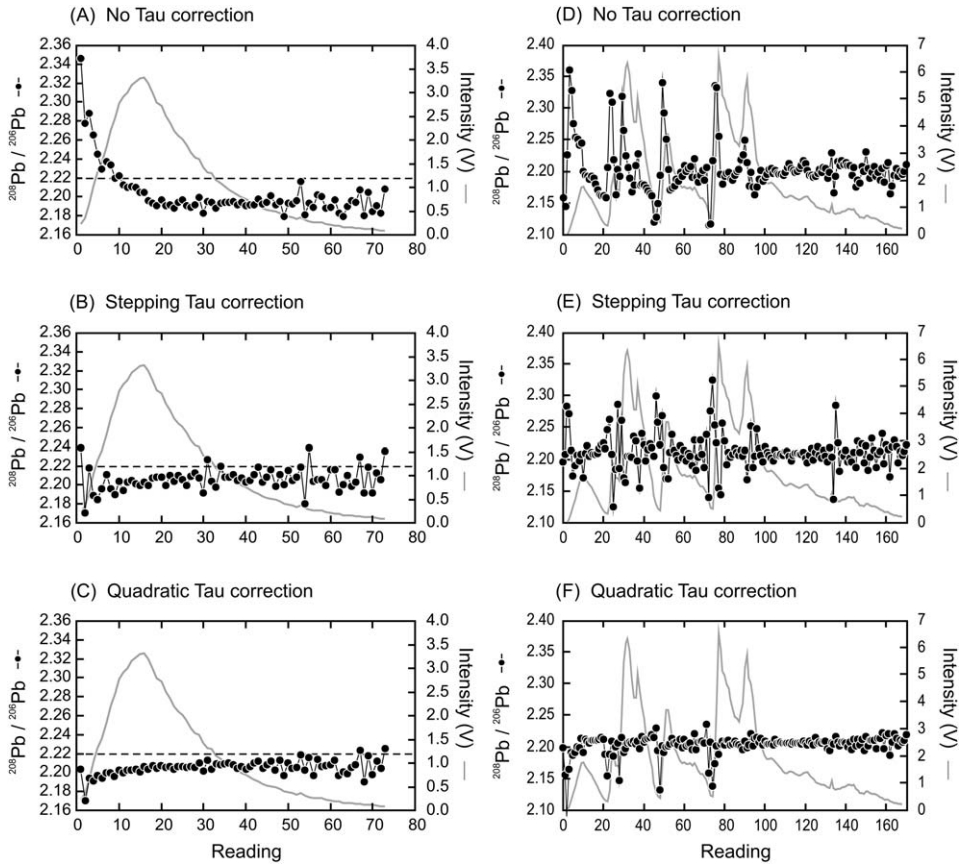


**Fig. 5** Plots of background-corrected Pb isotope ratios calculated for individual 0.2 s integration readings for two fluid inclusions measured by the straight ablation (A–C) and the stepwise opening (D–F) technique, uncorrected and corrected for amplifier response as indicated and detailed in text. Measured total Pb intensities are shown as the grey curves. Note that the isotope ratios (black dots) are plotted at the same scale. Dashed lines drawn at $^{208}Pb/^{206}Pb = 2.22$ in (A–C) are given for visual reference only. $^{208}Pb/^{206}Pb$ ratios not corrected for amplifier response show up to 10% scatter that is reduced through correction to *ca.* 1%.

integrated for $\Delta t$ s each, the $m^{th}$ reading, after correction based on the preceding $m - 1$ corrected readings, is

$$c_m = \left\{ m_m + \sum_{i=2}^{m-1} [(c_i - c_{i-1})\mathrm{resInt}(t_m - t_i)] - c_{m-1}\mathrm{resInt}(0) \right\} [1 - \mathrm{resInt}(0)]^{-1} \quad (3)$$

where $c$ refers to corrected readings, $m_m$ is the measured reading currently to be corrected, and resInt(…) is defined in eqn (2), with the values of the expressions in parentheses being substituted for $t$. For computational purposes the corrected readings together with their time stamps are stored in a rotating buffer of $m$ elements, $m$ depending on the time span over which an amplifier settling effect is resolvable in the data. We refer to this scheme as the *stepping tau correction*.

Eqn (3) can be applied on- or off-line and results in adequate correction of ratio *trends* caused by amplifier response effects (Fig. 5B). However, it cannot easily cope with noisy or spiky signal behaviour, introducing excess variance to ratio data (Fig. 5E). To better treat such fast intensity variations, we apply a quadratic scheme referred to as *quadratic tau correction* to derive a continuous function for approximation of beam intensities within a given integration interval based on the measured dataset. We begin by approximation of beam intensity $s$ as a function of time $t$ by a polynomial of second degree

$$s = ht^2 + kt + l, \quad (4)$$

which, for the $i^{th}$ reading, $s_i$, becomes

$$\mathrm{sInt}_i = h\left(t_i^2 + t_i\Delta t + \frac{(\Delta t)^2}{3}\right) + k\left(t_i + \frac{\Delta t}{2}\right) + l \quad (5)$$

when integrated from $t_i$ to $t_i + \Delta t$ and divided by $\Delta t$, with $t_i$ being the starting time of an integration interval of $\Delta t$ duration. For each reading $i$, the coefficients $h$, $k$ and $l$ are determined by solving a system of three such equations using the measured sInt and $t$ values at readings $i - 1$, $i$, and $i + 1$.

We will now use the signal variation given in eqn (4) as a base for deriving a function which can be applied for *tau* correction of *sequential* readings. The signal bias caused by signal variation during an interval $\Delta t$ at a time point located $t$ seconds after the start and outside of this interval can be written as a sum of

infinitesimal contributions from the signal variations during that interval, using the step response function implied in eqn (1):

$$\begin{aligned}\mathrm{res}(t) &= \sum_{j=1}^{n} a_j \sum_{i=2}^{m} \Big[h^*(i-1)^2(\Delta x)^2 + k^*(i-1)\Delta x \\ &\quad - h^* i^2 (\Delta x)^2 - k^* i \Delta x\Big] \mathrm{e}^{(i\Delta x - t)/\tau_j} \\ &= \Delta x \sum_{j=1}^{n} a_j \sum_{i=2}^{m} \big[h^* \Delta x (1-2i) - k^*\big] \mathrm{e}^{(i\Delta x - t)/\tau_j}. \end{aligned} \quad (6)$$

$a_j$, $\tau_j$ and $n$ are as defined for eqn (1), $h^*$ and $k^*$ are similar to $h$ and $k$ used in eqn (4), but calculated setting $t = 0$ for the start of the interval. The variable $i$ refers to the $i^{\mathrm{th}}$ infinitesimal signal step of $\Delta x$ duration, with $\sum_{i=1}^{m} \Delta x = \Delta t$ corresponding to the duration of the actual integration interval. Note that eqn (6) and the following equations are based on the real (unknown) beam intensities rather than on registered intensities modified by amplifier response. For $\Delta x \to 0$, eqn (6) can be replaced by the sum of the integrals

$$\mathrm{res}(t) = -\sum_{j=1}^{n} a_j \int_0^{\Delta t} \big(2h^* x + k^*\big) \mathrm{e}^{(x-t)/\tau_j} dx, \quad (7)$$

which gives

$$\mathrm{res}(t) = -\sum_{j=1}^{n} a_j \tau_j \mathrm{e}^{-t/\tau_j} \big\{ \big[2h^*(\Delta t - \tau_j) + k^*\big] \mathrm{e}^{\Delta t/\tau_j} + 2h^* \tau_j - k^* \big\}. \quad (8)$$

As for eqn (2), eqn (8) needs to be integrated to obtain the appropriate correction for a signal reading of $\Delta t$ duration starting $t$ seconds after the start of the interval responsible for the residual:

$$\begin{aligned}\mathrm{resInt}(t) = \frac{1}{\Delta t} \sum_{j=1}^{n} a_j \tau_j^2 \mathrm{e}^{-t/\tau_j} \big\{ \big[2h^*(\Delta t - \tau_j) + k^*\big] \mathrm{e}^{\Delta t/\tau_j} + 2h^* \tau_j \\ - k^* \big\} \big(\mathrm{e}^{-\Delta t/\tau_j} - 1\big) \end{aligned} \quad (9)$$

For eqn (6)–(9) to be valid, $t \geq \Delta t$ is an essential condition, *i.e.*, the integration interval to be corrected shall not overlap with the interval responsible for the residual. However, because beam variations within a given integration interval strongly affect the remaining part of the same interval, we need to derive a modified equation for this special case, using a similar approach, but observing variable integration boundaries. The result is

$$\begin{aligned}\mathrm{resInt}(0) = \frac{1}{\Delta t} \sum_{j=1}^{n} a_j \tau_j \big\{ \tau_j \big[2h^*(\Delta t - \tau_j) + k^* + \mathrm{e}^{-\Delta t/\tau_j} \big(2h^* \tau_j - k^*\big)\big] \\ - h^* \Delta^2 t - k^* \Delta t \big\} \end{aligned} \quad (10)$$

To then correct a set of $m$ continuous intensity readings $s_i$ for amplifier response, we start at reading $s_1$ (assuming that this reading is not biased by earlier signal variation), determine $h^*$ and $k^*$ (using readings 1, 2 and 3 in this special case) and derive the correction value for reading 1 by eqn (10). Eqn (9) and (10) are then applied to derive corrections for reading 2 and so on, summing and storing the correction values derived from all previous signal readings (by eqn (9)) and the internal correction (by eqn (10)) separately for each reading. When the full data array has been processed, the correction values (residuals) are subtracted from their respective readings. As the signal shifts resulting from these corrections are not yet accounted for by the algorithm, the procedure is iterated, but rather than using the measured readings, the stored correction values from the previous pass are used for input. Iteration is stopped, when the correction values fall below a given threshold. In contrast to the step-function based correction algorithm given by eqn (3), the current scheme can only be applied in off-line mode.

Fig. 5 illustrates the improvement achieved with the two *tau* correction procedures. Uncorrected inclusion signals produced by straight ablation technique show pronounced ratio evolution coincident with the rising part of the signal, which is characterized by the steep intensity gradient, while the slower signal decay during complete consumption of inclusion content has a much smaller effect (Fig. 5A). In contrast, the isotope ratios of the same inclusion corrected in stepping mode (Fig. 5B) show fairly uniform isotope ratios that tend to become somewhat heavier with progressive ablation. The quadratic *tau* correction results in an even smoother trend (Fig. 5C). We interpret this residual trend to heavier values to relate to subordinate laser-ablation and aerosol transport induced isotope fractionation varying by *ca.* 0.5% amu$^{-1}$. This trend, however, does not affect the accuracy of the final isotope ratios, if the measurements are properly evaluated (see below).

Signals of inclusions ablated with the stepwise opening technique are characterized by abrupt decays and rises when the laser beam is blanketed off for increasing laser beam diameter and by fluctuations stemming from irregularities in the ablation rate of the inclusion (Fig. 5D). This results in considerable scatter of the raw ratios, which is only moderately reduced by *tau* correction in stepping mode (Fig. 5E). Although the use of the quadratic *tau* correction scheme further reduces these ratio excursions (Fig. 5F), there still remains variability in isotope ratios which negatively affects data precision. The residual bias could either be due to a non-ideal behavior of amplifiers or inaccurate tracking of the ion signals using relatively long (0.2 s) integration timing, or both, enhanced by the ultrafast changes in signal intensity related to the stop-and-go process associated with laser-beam size increase. We cannot exclude the possibility, however, that there is also some contribution by mass fractionation effects arising from generation and transport of the laser aerosol. Moreover, this particular fluid inclusion analysis showed some breakout during beam size increase at reading 56; hence, ablation was not well controlled.

The examples given in Fig. 5 demonstrate that it is important to critically evaluate transient signal shapes during data reduction. Individual inclusions yield the best results if the transient signal is as smooth as possible, which is most likely achieved by straight ablation without deliberate interruptions for changing crater diameter. Robust data can thus be obtained on fluid inclusions, given that data evaluation is coupled with an appropriate *tau* correction.

 

### Mass bias correction strategies

Two different within-run mass bias correction strategies based on Tl were explored: (a) Tl provided from within the inclusion and (b) desolvated Tl admixed to the laser ablation aerosol. This section focuses exclusively on results obtained by the individual reading data reduction method, to better illustrate differences.

In strategy (a) synthetic inclusions containing a mixture of SRM 981 Pb and SRM 997 Tl were measured while aspirating a 1% $HNO_3$ blank solution through the desolvation unit. Because such inclusions serve as common source for both Pb and Tl, it should, in principle, be possible to correct for the combined effects of mass fractionation generated during inclusion ablation, aerosol transport, ion production, and ion extraction in the source of the ICP-MS (*i.e.*, instrumental mass bias *sensu stricto*), provided that Pb and Tl are affected in the same systematic fashion during fluid inclusion analysis and that the Pb–Tl fractionation parameters derived from SRM 610 glass ablation experiments are applicable to that process. The Pb–Tl fluid inclusion results listed in Table S2† demonstrate that the mean isotopic ratios of individual inclusions overlap at the 2 SD level with the nominal Pb isotope ratios of SRM 981,[31] with uncertainties as low as 0.2% 2 SD for $^{208}Pb/^{206}Pb$ and $^{207}Pb/^{206}Pb$ ratios, and *ca.* 0.4% for Pb isotope ratios normalized to mass 204. This compares favourably with external analytical precisions on fast transient signal measurement by MC-ICP-MS as reported by other studies (*e.g.*, for Hg: ≤4‰[40]). Scatter exceeding analytical error is apparent in some cases for data not corrected for amplifier response (*e.g.*, Pb–Tl fluid inclusions analyzed on Aug30-05; Table S2†) where individual Pb–Tl fluid inclusions were measured more precisely (down to 0.1% for all Pb isotope ratios), returning significantly different isotope ratios for individual fluid inclusions that sometimes also deviate from the reference values (*e.g.*, Pb–Tl_FI-5_Aug30-05). The distribution of Tl in the analyzed fluid inclusions is heterogeneous, as revealed by the Pb/Tl intensity ratios monitored during the analyses. Most inclusions showed some decoupling of the Tl signal structure from that of the Pb isotopes, possibly resulting from ablation of tiny Tl-enriched crystals existing in the inclusions or early release of Tl from the inclusion (Fig. 2A and B). The precision obtained, in particular for smaller inclusions, also suffers from low Tl signals which do not permit precise mass bias correction on a reading-to-reading basis.

For the smaller and flatter Pb-only inclusions, there is only a limited dataset with adequate analytical precision for evaluation of strategy (b) (Table S2†). Even for these inclusions, however, accurate results can be obtained by adding the Tl required for mass bias correction *via* desolvating nebulisation up-torch to the LA aerosol generated from Pb-only inclusions (Table 4 and below). Because of the low average intensities on mass 204 ($2–6 \times 10^{-14}$ A) obtained for these smaller inclusions, the $^{20x}Pb/^{204}Pb$ ratios measured on individual inclusions are less precise than those measured for the larger Pb–Tl inclusions.

In order to further test the applicability of the Tl admixture approach, an assemblage of 20–30 μm sized Pb–Tl inclusions ($n = 12$) was analyzed by addition of Tl from the desolvating unit, exactly as done for the Pb-only inclusions. These data (Table 4) reveal an overall better inclusion-to-inclusion reproducibility for $^{208}Pb/^{206}Pb$ and $^{207}Pb/^{206}Pb$ ratios at within-run precisions even better than those obtained for larger Pb–Tl inclusions when analyzed without Tl admixture (this also holds for the Pb–Tl fluid inclusion data collected during the same session on Aug30, Table S2†). This supports our view that inclusion-to-inclusion analytical reproducibility can suffer from limitations on mass bias correction imposed by low-intensity fluid inclusion Tl signals and by non-uniform distribution of Tl in our synthetic Pb–Tl fluid inclusions. Most importantly, however, our tests demonstrate that accurate data can be obtained for the Pb isotope analysis of an individual fluid inclusion and that these tests do not resolve any disadvantage in admixing desolvated Tl to the laser ablation aerosol for mass bias correction.

### Individual reading *versus* entire signal integration

To further investigate ablation trends and to better define a strategy for choosing interval limits for fast transient signal analysis, the isotope ratios calculated for individual 0.2 s integration intervals from a set of inclusions with Tl admixed from a desolvator (Table 4) were averaged over four types of signal intervals (Fig. 6A), (1) first part of the signal covering the signal rise from the baseline to the peak, (2) second part of the signal from the peak down to the baseline, (3) a "wide" interval, comprising both the first and the second parts of the signal, and (4) a "widest best-precision" interval which selects the segment optimizing the internal precision of the $^{208}Pb/^{206}Pb$ and $^{207}Pb/^{206}Pb$ ratios while maintaining the integration interval as large as possible. The results plotted in Fig. 6B demonstrate that $^{208}Pb/^{206}Pb$ in the first part of the ablation at rising signal intensity is generally significantly heavier, while the second half of the signal at dropping signal intensity the ratio tends to be lighter than the averages calculated for the "wide" and the "widest best-precision" intervals. The latter most closely approximate the true value. This pattern becomes considerably modified for *tau*-corrected data (bottom graph), with a slight predominance of light Pb during the first part of the signal trace and heavier Pb during the second part (as observed for an individual inclusion analysis, Fig. 5B and C). The ratios with $^{204}Pb$ in the denominator are not shown, because they are not precise enough to reveal the trends.

The given examples demonstrate that one needs to integrate the entire transient signal, which can be done in essentially two ways, named here the *individual reading integration* method and the *bulk signal integration* method. Using the individual reading integration method, each reading is weighed equally for deriving the final isotopic ratio of the sample. This approach may be inadequate for the analysis of highly transient signals, where signal intensities may vary by more than two orders of magnitude during sample analysis, because low-intensity readings yield ratios of poorer precision compared to high-intensity readings. Cutting off the low-intensity wings of the transient signals altogether is also not desirable, because such portions of the ablation signal are often highly fractionated and their omission can bias the final result (compare Fig. 5 and 6).

Intensity-weighted average isotope ratios of transient signals are expected to be more representative, because low-intensity and possibly highly fractionated and/or imprecise readings exert less weight in averaging. This is partially equivalent to *bulk signal integration*, *i.e.*, to the summation of signal intensities over

**Table 4** LA-ICP-MS Pb isotope results of individual synthetic fluid inclusions analysed in session August 30, 2005, on Nu Plasma 1700[a]

| | FI chip number | FI size/ μm | Ablation quality[b] | $^{208}Pb/^{206}Pb$ | Error abs.[c] | # of readings | $^{207}Pb/^{206}Pb$ | Error abs.[c] | # of readings | $^{206}Pb/^{204}Pb$ | Error abs.[c] | # of readings | $^{207}Pb/^{204}Pb$ | Error abs.[c] | # of readings | $^{208}Pb/^{204}Pb$ | Error abs.[c] | # of readings |
|---|---|---|---|---|---|---|---|---|---|---|---|---|---|---|---|---|---|---|
| SRM 981 reference values (Baker *et al.*[31]) | | | | 2.1678 | | | 0.9149 | | | 16.94 | | | 15.50 | | | 36.73 | | |
| (A) August 30, 2005: results obtained by the individual time slice integration method, not corrected for amplifier response | | | | | | | | | | | | | | | | | | |
| Pb_FI-1_Aug30-05 | C1 | 35 | +++ | 2.1645 | 0.0023 | 47 of 50 | 0.9138 | 0.0008 | 47 of 50 | 16.98 | 0.06 | 46 of 50 | 15.54 | 0.05 | 47 of 50 | 36.82 | 0.13 | 48 of 50 |
| *Pb_FI-2_Aug30-05* | *C1* | 35 | *Exploded* | *2.1610* | 0.0042 | *36 of 39* | *0.9124* | 0.0013 | *37 of 39* | *17.05* | 0.09 | *37 of 39* | *15.57* | 0.09 | *37 of 39* | *36.90* | 0.23 | *37 of 39* |
| *Pb_FI-3_Aug30-05* | *C1* | 35 | *Exploded* | *2.1609* | 0.0028 | *38 of 40* | *0.9130* | 0.0007 | *38 of 40* | *16.96* | 0.02 | *39 of 40* | *15.50* | 0.02 | *37 of 40* | *36.67* | 0.07 | *39 of 40* |
| Pb_FI-4_Aug30-05 | C1 | 30 | +++ | 2.1644 | 0.0020 | 69 of 74 | 0.9138 | 0.0007 | 70 of 74 | 16.90 | 0.09 | 69 of 74 | 15.46 | 0.09 | 70 of 74 | 36.65 | 0.21 | 69 of 74 |
| Pb_FI-5_Aug30-05 | C1 | 60 | +++ | 2.1664 | 0.0010 | 127 of 135 | 0.9143 | 0.0004 | 128 of 135 | 16.98 | 0.05 | 129 of 135 | 15.53 | 0.05 | 129 of 135 | 36.83 | 0.11 | 128 of 135 |
| Pb_FI-6_Aug30-05 | C3 | 30 | +++ | 2.1673 | 0.0021 | 85 of 87 | 0.9146 | 0.0006 | 83 of 87 | 16.99 | 0.07 | 81 of 87 | 15.55 | 0.06 | 80 of 87 | 36.85 | 0.16 | 82 of 87 |
| Pb_FI-7_Aug30-05 | C3 | 70 | +++ | 2.1681 | 0.0009 | 194 of 204 | 0.9147 | 0.0004 | 194 of 204 | 16.98 | 0.05 | 191 of 204 | 15.54 | 0.04 | 192 of 204 | 36.83 | 0.10 | 191 of 204 |
| Pb_FI-8_Aug30-05 | C3 | 30 | +++ | 2.1665 | 0.0023 | 70 of 75 | 0.9142 | 0.0006 | 70 of 75 | 16.86 | 0.12 | 68 of 75 | 15.45 | 0.11 | 70 of 75 | 36.55 | 0.27 | 70 of 75 |
| Pb–Tl_FI-9_Aug30-05 | A4 | 30 | ++(+) | 2.1657 | 0.0021 | 70 of 73 | 0.9140 | 0.0007 | 71 of 73 | 16.91 | 0.06 | 69 of 73 | 15.47 | 0.05 | 70 of 73 | 36.66 | 0.13 | 70 of 73 |
| Pb–Tl_FI-10_Aug30-05 | A4 | 35 | +++ | 2.1676 | 0.0013 | 202 of 215 | 0.9146 | 0.0006 | 202 of 215 | 16.95 | 0.07 | 202 of 215 | 15.51 | 0.06 | 201 of 215 | 36.79 | 0.15 | 203 of 215 |
| Pb–Tl_FI-11_Aug30-05 | A4 | 25 | ++ | 2.1657 | 0.0018 | 93 of 99 | 0.9145 | 0.0007 | 93 of 99 | 16.95 | 0.10 | 94 of 99 | 15.51 | 0.09 | 92 of 99 | 36.69 | 0.19 | 92 of 99 |
| Pb–Tl_FI-12_Aug30-05 | A4 | 40 | +++ | 2.1677 | 0.0017 | 113 of 117 | 0.9140 | 0.0007 | 110 of 117 | 17.00 | 0.06 | 108 of 117 | 15.53 | 0.06 | 109 of 117 | 36.83 | 0.14 | 109 of 117 |
| Pb–Tl_FI-13_Aug30-05 | A4 | 25 | +++ | 2.1691 | 0.0014 | 97 of 103 | 0.9152 | 0.0005 | 98 of 103 | 16.96 | 0.06 | 97 of 103 | 15.53 | 0.05 | 96 of 103 | 36.81 | 0.12 | 96 of 103 |
| Pb–Tl_FI-14_Aug30-05 | A4 | 35 | +++ | 2.1671 | 0.0019 | 74 of 78 | 0.9146 | 0.0005 | 75 of 78 | 16.90 | 0.07 | 72 of 78 | 15.46 | 0.06 | 73 of 78 | 36.60 | 0.15 | 73 of 78 |
| Pb–Tl_FI-15_Aug30-05 | A4 | 45 | +++ | 2.1664 | 0.0023 | 66 of 68 | 0.9146 | 0.0007 | 65 of 68 | 16.99 | 0.07 | 62 of 68 | 15.53 | 0.06 | 61 of 68 | 36.81 | 0.15 | 61 of 68 |
| Pb–Tl_FI-16_Aug30-05 | A4 | 22 | +++ | 2.1676 | 0.0019 | 89 of 91 | 0.9149 | 0.0006 | 87 of 91 | 17.03 | 0.07 | 83 of 91 | 15.59 | 0.06 | 82 of 91 | 36.92 | 0.14 | 81 of 91 |
| Pb–Tl_FI-17_Aug30-05 | A4 | 25 | +++ | 2.1691 | 0.0018 | 92 of 98 | 0.9151 | 0.0006 | 92 of 98 | 16.91 | 0.11 | 92 of 98 | 15.46 | 0.10 | 91 of 98 | 36.65 | 0.23 | 91 of 98 |
| Pb–Tl_FI-18_Aug30-05 | A4 | 50 | ++(+) | 2.1667 | 0.0021 | 80 of 86 | 0.9146 | 0.0008 | 79 of 86 | 16.99 | 0.14 | 82 of 86 | 15.54 | 0.13 | 82 of 86 | 36.83 | 0.31 | 82 of 86 |
| Pb–Tl_FI-19_Aug30-05 | A4 | 30 | +++ | 2.1686 | 0.0014 | 114 of 116 | 0.9155 | 0.0005 | 109 of 116 | 16.93 | 0.08 | 108 of 116 | 15.51 | 0.07 | 108 of 116 | 36.74 | 0.18 | 109 of 116 |
| Pb–Tl_FI-20_Aug30-05 | A4 | 30 | +++ | 2.1675 | 0.0019 | 76 of 80 | 0.9147 | 0.0007 | 75 of 80 | 16.89 | 0.07 | 74 of 80 | 15.45 | 0.07 | 74 of 80 | 36.62 | 0.17 | 74 of 80 |
| **Average** | | | | 2.1670 | | | 0.9145 | | | 16.95 | | | 15.51 | | | 36.75 | | |
| **2 SD (abs.)** | | | | 0.0027 | | | 0.0010 | | | 0.09 | | | 0.08 | | | 0.21 | | |
| **2 SD (ppm)** | | | | 1252 | | | 1048 | | | 5495 | | | 5442 | | | 5817 | | |
| **2 SE (abs.)** | | | | 0.0006 | | | 0.0002 | | | 0.02 | | | 0.02 | | | 0.05 | | |
| **2 SE (ppm)** | | | | 295 | | | 247 | | | 1295 | | | 1283 | | | 1371 | | |

**Table 4** (*Contd.*)

| | FI chip number | FI size/ μm | Ablation quality[b] | $^{208}Pb/^{206}Pb$ | Error abs.[c] | # of readings | $^{207}Pb/^{206}Pb$ | Error abs.[c] | # of readings | $^{206}Pb/^{204}Pb$ | Error abs.[c] | # of readings | $^{207}Pb/^{204}Pb$ | Error abs.[c] | # of readings | $^{208}Pb/^{204}Pb$ | Error abs.[c] | # of readings |
|---|---|---|---|---|---|---|---|---|---|---|---|---|---|---|---|---|---|---|
| (B) August 30, 2005: results obtained by the bulk signal integration method, corrected for amplifier response | | | | | | | | | | | | | | | | | | |
| Pb_FI-1_Aug30-05 | C1 | 35 | +++ | 2.1678 | 0.0011 | — | 0.9145 | 0.0005 | — | 16.99 | 0.07 | — | 15.54 | 0.06 | — | 36.84 | 0.15 | — |
| Pb_FI-2_Aug30-05 | C1 | 35 | Exploded | 2.1661 | 0.0016 | — | 0.9134 | 0.0008 | — | 17.04 | 0.14 | — | 15.57 | 0.13 | — | 36.91 | 0.30 | — |
| Pb_FI-3_Aug30-05 | C1 | 35 | Exploded | 2.1678 | 0.0008 | — | 0.9146 | 0.0003 | — | 16.95 | 0.02 | — | 15.50 | 0.02 | — | 36.74 | 0.04 | — |
| Pb_FI-4_Aug30-05 | C1 | 30 | +++ | 2.1656 | 0.0013 | — | 0.9137 | 0.0006 | — | 16.95 | 0.10 | — | 15.49 | 0.09 | — | 36.72 | 0.21 | — |
| Pb_FI-5_Aug30-05 | C1 | 60 | +++ | 2.1679 | 0.0009 | — | 0.9145 | 0.0004 | — | 16.97 | 0.05 | — | 15.52 | 0.05 | — | 36.78 | 0.12 | — |
| Pb_FI-6_Aug30-05 | C3 | 30 | +++ | 2.1676 | 0.0011 | — | 0.9146 | 0.0005 | — | 16.96 | 0.07 | — | 15.51 | 0.07 | — | 36.76 | 0.16 | — |
| Pb_FI-7_Aug30-05 | C3 | 70 | +++ | 2.1683 | 0.0009 | — | 0.9148 | 0.0004 | — | 16.97 | 0.06 | — | 15.53 | 0.06 | — | 36.81 | 0.13 | — |
| Pb_FI-8_Aug30-05 | C3 | 30 | +++ | 2.1672 | 0.0013 | — | 0.9143 | 0.0006 | — | 16.89 | 0.10 | — | 15.45 | 0.09 | — | 36.61 | 0.22 | — |
| Pb–Tl_FI-9_Aug30-05 | A4 | 30 | ++(+) | 2.1687 | 0.0010 | — | 0.9147 | 0.0005 | — | 16.92 | 0.06 | — | 15.48 | 0.06 | — | 36.70 | 0.14 | — |
| Pb–Tl_FI-10_Aug30-05 | A4 | 35 | +++ | 2.1684 | 0.0010 | — | 0.9148 | 0.0005 | — | 16.93 | 0.09 | — | 15.49 | 0.08 | — | 36.72 | 0.19 | — |
| Pb–Tl_FI-11_Aug30-05 | A4 | 25 | ++ | 2.1675 | 0.0013 | — | 0.9146 | 0.0006 | — | 16.96 | 0.10 | — | 15.51 | 0.09 | — | 36.76 | 0.21 | — |
| Pb–Tl_FI-12_Aug30-05 | A4 | 40 | +++ | 2.1680 | 0.0010 | — | 0.9145 | 0.0005 | — | 16.99 | 0.08 | — | 15.54 | 0.07 | — | 36.83 | 0.16 | — |
| Pb–Tl_FI-13_Aug30-05 | A4 | 25 | +++ | 2.1691 | 0.0009 | — | 0.9150 | 0.0004 | — | 16.97 | 0.05 | — | 15.53 | 0.05 | — | 36.81 | 0.12 | — |
| Pb–Tl_FI-14_Aug30-05 | A4 | 35 | +++ | 2.1683 | 0.0011 | — | 0.9149 | 0.0005 | — | 16.93 | 0.07 | — | 15.49 | 0.07 | — | 36.72 | 0.15 | — |
| Pb–Tl_FI-15_Aug30-05 | A4 | 45 | +++ | 2.1687 | 0.0010 | — | 0.9149 | 0.0005 | — | 17.00 | 0.06 | — | 15.55 | 0.06 | — | 36.87 | 0.13 | — |
| Pb–Tl_FI-16_Aug30-05 | A4 | 22 | +++ | 2.1681 | 0.0011 | — | 0.9149 | 0.0005 | — | 17.00 | 0.08 | — | 15.55 | 0.07 | — | 36.85 | 0.17 | — |
| Pb–Tl_FI-17_Aug30-05 | A4 | 25 | +++ | 2.1695 | 0.0013 | — | 0.9151 | 0.0007 | — | 16.93 | 0.10 | — | 15.49 | 0.10 | — | 36.72 | 0.22 | — |
| Pb–Tl_FI-18_Aug30-05 | A4 | 50 | ++(+) | 2.1676 | 0.0017 | — | 0.9147 | 0.0009 | — | 16.98 | 0.16 | — | 15.53 | 0.15 | — | 36.81 | 0.34 | — |
| Pb–Tl_FI-19_Aug30-05 | A4 | 30 | +++ | 2.1685 | 0.0011 | — | 0.9152 | 0.0005 | — | 16.95 | 0.08 | — | 15.51 | 0.07 | — | 36.75 | 0.17 | — |
| Pb–Tl_FI-20_Aug30-05 | A4 | 30 | +++ | 2.1684 | 0.0011 | — | 0.9147 | 0.0006 | — | 16.88 | 0.09 | — | 15.44 | 0.08 | — | 36.61 | 0.20 | — |
| **Average** | | | | 2.1681 | | | 0.9147 | | | 16.95 | | | 15.51 | | | 36.76 | | |
| **2 SD (abs.)** | | | | 0.0017 | | | 0.0007 | | | 0.07 | | | 0.06 | | | 0.15 | | |
| **2 SD (ppm)** | | | | 766 | | | 761 | | | 4004 | | | 4110 | | | 4028 | | |
| **2 SE (abs.)** | | | | 0.0004 | | | 0.0002 | | | 0.02 | | | 0.02 | | | 0.03 | | |
| **2 SE (ppm)** | | | | 181 | | | 179 | | | 944 | | | 969 | | | 949 | | |

[a] Values in italics were excluded from calculation of averages because fluid inclusion ablation was not well controlled. [b] Quality of fluid inclusion ablation as visually judged on monitor screen (+++ = excellent; ++ = acceptable; + = poor). [c] Refers to absolute uncertainties expressed for dataset A as 2 SE measurement errors, for dataset B as the 95% confidence limit calculated following Baxter *et al.*[26]

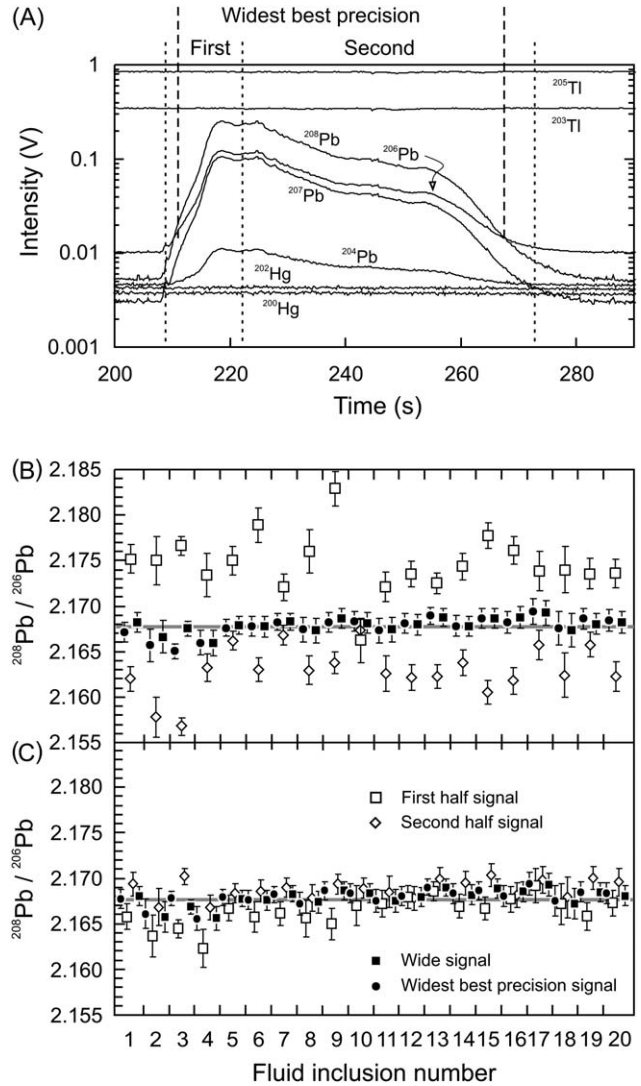


**Fig. 6** Lead isotope ratios from 20 fluid inclusions integrated across different segments of the transient signals using the individual reading integration method. Internal mass bias correction is based on Tl admixed from a desolvator. (A) An example of intervals chosen for integration; "First" refers to first part of the signal trace, "Second" to the second part, wide encompasses both the first and second parts of the signal, and the "widest best precision" is calculated as explained in the text. (B) Pb isotope data without correction for amplifier response. Substantially elevated $^{208}Pb/^{206}Pb$ ratios are observed for the first part of the signal, while the second part is generally lighter than both the "wide" and the "widest best-precision" signal averages, which overlap for a given inclusion ablation. (C) The same data corrected for amplifier response as detailed in the text. Although considerably reduced in magnitude, there remains a systematic offset between the averages of the first and second half of the fluid inclusion signals for several inclusion analyses, interpreted to relate to isotope fractionation at the laser ablation site (compare Fig. 5B and C). Error bars are 95% confidence limit following Baxter *et al.*[26]

a chosen signal section (*e.g.*, Evans *et al.*[40]) before applying the data reduction scheme to these integrated signal values. A drawback of this scheme is that information about isotope ratio evolution across the transient signal as addressed above is lost and that no information on internal errors can directly be gained from the data. Minimum estimates for the uncertainty of isotope ratios as calculated by the bulk signal integration method can, however, be obtained from Gaussian combination of ion statistics and baseline noise. Adopting an average value of $3.2 \times 10^{-16}$ A (1 SD of baseline readings integrated for 1 s) for the latter, we have generated estimates for the uncertainties listed in Table 4 using Monte Carlo techniques. Note that these uncertainties do not include systematic and random errors associated with *tau* correction.

Fig. 7 compares three datasets of the same 20 fluid inclusion analyses reduced by the individual reading integration method (i) and the bulk signal integration method (ii and iii), each applied to the same number of readings per fluid inclusion. Methods (i) and (ii) use data not corrected for amplifier response, while for (iii) they were corrected using the stepping *tau* correction scheme. The most prominent difference is the increase in accuracy when

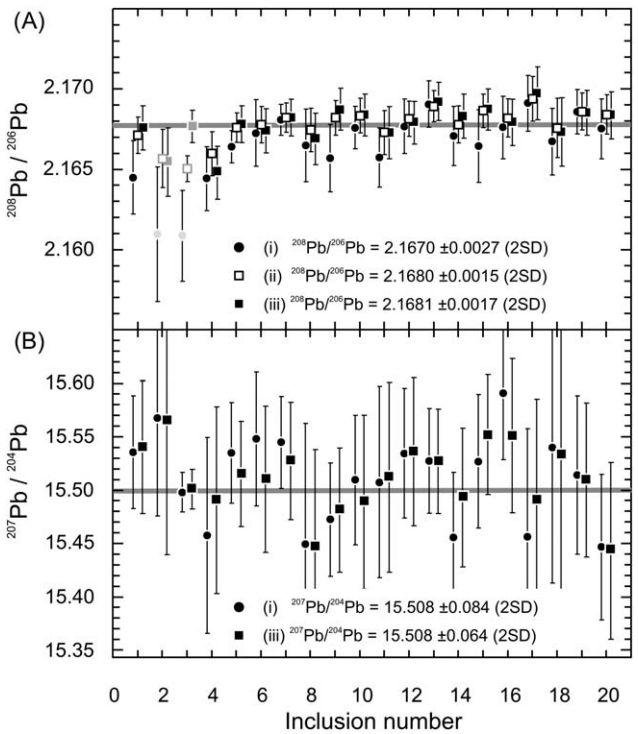


**Fig. 7** External reproducibility plots for $^{208}Pb/^{206}Pb$ (A) and $^{207}Pb/^{204}Pb$ (B) ratios for 20 individual fluid inclusion (20–25 μm diameter) analyses using aspirated Tl for mass bias correction. Grey data points were discarded from the averaged dataset, due to uncontrolled fluid inclusion ablation, which may generate precise measurements of unconstrained accuracy. Thick grey lines represent nominal values for SRM 981.[31] Black dots (i) represent data obtained by the individual reading integration method using the widest best precision interval (dataset (A) in Table 4) with 2 SE measurement uncertainties. Open (ii) and filled (iii) black squares represent isotope ratios calculated by the bulk signal integration method, with a lower limit of uncertainty estimated from a Gaussian combination of ion statistics and baseline noise. Filled black squares (iii) are calculated using data corrected for amplifier response (dataset (B) in Table 4), while open squares (ii) represent uncorrected data. Data obtained by the bulk signal integration method (ii and iii) are significantly more accurate and scatter less for isotope ratios normalized to $^{206}Pb$ while its effect is not so obvious for isotope ratios normalized to $^{204}Pb$, due to the low precision of the $^{204}Pb$ measurements. See text for explanation.

 

using the bulk signal integration method, even without *tau* correction (compare (i) and (ii) in Fig. 7A). In addition, the two outliers in the $^{208}Pb/^{206}Pb$ ratio resulting from poorly controlled fluid inclusion ablation can no longer be deemed outliers when using the bulk signal integration method with *tau* correction; hence, the effect of poorly controlled fluid inclusion ablation may in part be mitigated by use of the summed signal intensities of the entire signal interval. The same improvement is not observed for ratios normalized to mass 204 (Fig. 7B), due to limited measurement precision on mass 204.

The best accuracy (Fig. 7) for a fast transient signal analysis is obtained by the bulk signal integration method (see also Cottle *et al.*[19]). Given the limitations in transient data recording that, to our knowledge, apply to all currently used MC-ICP-MS instruments to variable degree, our findings conform to the notion that successful methods of transient signal analysis rely on integration schemes that use most of the transient signal, *i.e.*, essentially the entire sample, for isotope ratio determination. For fluid inclusions specifically, this requires controlled ablation by the straight ablation technique and recording of the entire inclusion content. Fluid inclusions vary in size (thus in total amount of Pb available for analysis) and geometries (translating to different transient signal shapes); hence, the quality of individual fluid inclusion analyses varies significantly. The laser ablation and aerosol transport processes together with the commonly sub-ng amounts of Pb available for analysis likely dominate the overall analytical uncertainty of an individual fluid inclusion for *tau* corrected signal recordings. Therefore, the Pb isotope composition of the fluid is best represented by the uncertainty-weighted average isotopic composition calculated from a series of individually analyzed fluid inclusions that belong to a fluid inclusion assemblage (see Pettke[9] for more information).

### An example of natural fluid inclusions

Data obtained on samples of fluid inclusions from porphyry-type ore deposits demonstrate that the analytical precision obtained on natural samples can be even better than that documented above for our fluid inclusion standards (Table 5). Fig. 8 illustrates the data obtained on the Nu Plasma instrument. The reproducibility obtained for two inclusion assemblages (*i.e.*, coevally entrapped individual inclusions on a single healed microfracture in quartz, representing individual samples of an isotopically uniform fluid[9]) from one vein quartz sample serves as a good example for the data quality achievable for fluid inclusion Pb isotope analysis. Here, the inclusion-to-inclusion reproducibility is *ca.* 0.05% (2 SD; $n = 11$) for $^{208}Pb/^{206}Pb$ and $^{207}Pb/^{206}Pb$, and *ca.* 0.13% for Pb isotope ratios with mass 204 in the denominator (data calculated by bulk signal integration). The uncertainties expressed as two standard errors of the mean of the 11 inclusion analyses are *ca.* 0.016 and *ca.* 0.04%, respectively.

Based on our results obtained on synthetic fluid inclusions, these analyses are considered to be accurate within their calculated precisions. Potential interferences in chemically complex natural fluid inclusions may include chloride ions of rare earth elements (REE, lanthanide group) or polyatomic argide ions. Concentrations of middle to heavy REE are low in normal crustal fluids, and the analysis of the SRM 610 glass containing approximately 440 μg $g^{-1}$ each of REE did not reveal such problems. The synthetic fluid inclusion standards are well suited for evaluating the production of metal-hydride ions or peak tailing effects, and such problems have not been identified in the current dataset. In some geological environments, Hg may represent a significant component, in which case the measured $^{202}Hg/^{200}Hg$ ratio can be used to characterize mass bias for interference correction at mass 204. Mercury interference correction on mass 204 based on the Tl proxy as used in this study is considered robust for fluid inclusions when Hg is a rare component (*i.e.*, $^{202}Hg/^{204}Pb < 0.1$). Isobaric interference by $WO^+$ ions on $^{202}Hg$, on the other hand, could potentially result in an inappropriate Hg interference correction but, typically, W concentrations in fluid inclusions are rather low except for hot magmatic–hydrothermal fluids originating from highly fractionated silicate melts associated with Sn–W ore deposits (*e.g.*, Audétat *et al.*[44]). In such a case, $^{201}Hg$ could be used for mass bias correction instead, unless interfered by $ReO^+$, which is unlikely to be present in significant concentrations in high-salinity brine inclusions. $^{201}Hg$ may thus be an alternative choice for Hg interference correction for specific natural samples. It is thus concluded that accurate data can be obtained from the analysis of individual natural fluid inclusions even for complex solution compositions (*e.g.*, Pettke *et al.*[21]).

## Concluding remarks

The MC-ICP-MS analytical procedures for Pb isotope ratios recorded in transient data acquisition mode are developed here for fast transient signals as produced by laser ablation of individual fluid inclusions. Extensive testing demonstrates:

- Differences in amplifier response among Faraday detectors are often not adequately accounted for by commercial instruments. We thus present rigorous *tau* correction schemes and demonstrate their success.
- To obtain accurate isotope ratios, transient signals need to be integrated and processed as an entity.
- Signals integrated using the individual reading method on *tau*-corrected data reveal that Pb isotope ratios become heavier with progressive fluid inclusion ablation, which we ascribe to laser-ablation induced isotope fractionation. The magnitude of this fractionation is small and not relevant for the analyses of individual fluid inclusions presented here.
- Results for an individual fluid inclusion are best calculated using the bulk signal integration method, whereby high-intensity readings have correspondingly greater weight in defining the overall isotope ratios.
- Mass bias correction based on Tl admixed as desolvated aerosol to the laser ablation aerosol can generate highly accurate data.
- Individual fluid inclusions are best analyzed by the straight ablation technique; stepwise opening causes fast changes in signal intensities requiring larger and less-precise corrections for amplifier response.
- Interferences typically pose no limitations to data accuracy in our application to saline and Pb-rich (0.1 wt% Pb) magmatic–hydrothermal fluid inclusions.

The external precision achieved on MC-ICP-MS instruments for repetitive analysis of SRM 610 glass is shown to converge to ±0.011% (2 SD) for $^{208}Pb/^{206}Pb$ and $^{207}Pb/^{206}Pb$ ratios and to

**Table 5** Data for two natural fluid inclusion assemblages from the porphyry copper deposit at Rosia Poieni[a]

| Sample | FI size/μm | Ablation quality[b] | $^{208}Pb/^{206}Pb$ | CI 95%[c] | $^{207}Pb/^{206}Pb$ | CI 95%[c] | $^{206}Pb/^{204}Pb$ | CI 95% [c] | $^{207}Pb/^{204}Pb$ | CI 95%[c] | $^{208}Pb/^{204}Pb$ | CI 95%[c] |
|---|---|---|---|---|---|---|---|---|---|---|---|---|
| Individual reading integration; widest best precision interval | | | | | | | | | | | | |
| 050706_RP_FI-1 | 30 | +++ | 2.05768 | 0.00111 | 0.83576 | 0.00070 | 18.648 | 0.027 | 15.603 | 0.020 | 38.369 | 0.054 |
| 050706_RP_FI-2 | 30 | +++ | 2.05884 | 0.00114 | 0.83647 | 0.00105 | 18.644 | 0.026 | 15.603 | 0.016 | 38.379 | 0.047 |
| 050706_RP_FI-3 | 35 | +++ | 2.05884 | 0.00087 | 0.83634 | 0.00047 | 18.649 | 0.019 | 15.601 | 0.017 | 38.390 | 0.042 |
| 050706_RP_FI-4 | 40 | +++ | 2.05874 | 0.00100 | 0.83597 | 0.00048 | 18.655 | 0.017 | 15.603 | 0.016 | 38.414 | 0.043 |
| 050706_RP_FI-5 | 40 | +++ | 2.05936 | 0.00116 | 0.83671 | 0.00071 | 18.644 | 0.040 | 15.603 | 0.033 | 38.396 | 0.088 |
| 050706_RP_FI-6 | 30 | +++ | 2.05949 | 0.00101 | 0.83640 | 0.00073 | 18.657 | 0.021 | 15.609 | 0.016 | 38.414 | 0.049 |
| 050706_RP_FI-7 | 50 | ++(+) | 2.05998 | 0.00107 | 0.83687 | 0.00077 | 18.671 | 0.021 | 15.621 | 0.016 | 38.461 | 0.049 |
| *050706_RP_FI-8* | 75 | ++ | *2.05841* | *0.00068* | *0.83585* | *0.00033* | *18.674* | *0.012* | *15.615* | *0.009* | *38.442* | *0.025* |
| 050706_RP_FI-9 | 35 | +++ | 2.05912 | 0.00115 | 0.83653 | 0.00105 | 18.635 | 0.021 | 15.596 | 0.013 | 38.367 | 0.041 |
| 050706_RP_FI-10 | 40 | +++ | 2.06027 | 0.00103 | 0.83694 | 0.00095 | 18.674 | 0.021 | 15.625 | 0.013 | 38.472 | 0.042 |
| 050706_RP_FI-11 | 35 | +++ | 2.05849 | 0.00079 | 0.83630 | 0.00038 | 18.641 | 0.020 | 15.593 | 0.015 | 38.363 | 0.043 |
| 050706_RP_FI-12 | 35 | ++(+) | 2.05917 | 0.00119 | 0.83626 | 0.00081 | 18.631 | 0.029 | 15.589 | 0.020 | 38.349 | 0.057 |
| **Average** | | | **2.05909** | | **0.83641** | | **18.650** | | **15.604** | | **38.397** | |
| **2 SD (abs.)** | | | **0.00141** | | **0.00071** | | **0.027** | | **0.022** | | **0.080** | |
| **2 SD (ppm)** | | | **686** | | **848** | | **1466** | | **1391** | | **2072** | |
| **2 SE (abs.)** | | | **0.00043** | | **0.00021** | | **0.008** | | **0.007** | | **0.024** | |
| **2 SE (ppm)** | | | **207** | | **256** | | **442** | | **419** | | **625** | |
| Bulk signal integration; widest best precision interval | | | | | | | | | | | | |
| 050706_RP_FI-1 | 30 | +++ | 2.05857 | 0.00088 | 0.83667 | 0.00029 | 18.650 | 0.018 | 15.604 | 0.016 | 38.391 | 0.042 |
| 050706_RP_FI-2 | 30 | +++ | 2.05890 | 0.00089 | 0.83670 | 0.00029 | 18.644 | 0.016 | 15.600 | 0.014 | 38.386 | 0.040 |
| 050706_RP_FI-3 | 35 | +++ | 2.05908 | 0.00083 | 0.83669 | 0.00028 | 18.649 | 0.016 | 15.603 | 0.015 | 38.398 | 0.039 |
| 050706_RP_FI-4 | 40 | +++ | 2.05927 | 0.00091 | 0.83665 | 0.00028 | 18.658 | 0.014 | 15.610 | 0.013 | 38.421 | 0.038 |
| 050706_RP_FI-5 | 40 | +++ | 2.05900 | 0.00098 | 0.83687 | 0.00031 | 18.641 | 0.022 | 15.600 | 0.019 | 38.381 | 0.051 |
| 050706_RP_FI-6 | 30 | +++ | 2.05988 | 0.00089 | 0.83696 | 0.00028 | 18.648 | 0.014 | 15.608 | 0.013 | 38.413 | 0.037 |
| 050706_RP_FI-7 | 50 | ++(+) | 2.06038 | 0.00089 | 0.83708 | 0.00028 | 18.665 | 0.013 | 15.625 | 0.012 | 38.457 | 0.036 |
| *050706_RP_FI-8* | 75 | ++ | *2.05859* | *0.00072* | *0.83621* | *0.00025* | *18.668* | *0.010* | *15.611* | *0.009* | *38.429* | *0.025* |
| 050706_RP_FI-9 | 35 | +++ | 2.05939 | 0.00085 | 0.83689 | 0.00027 | 18.640 | 0.012 | 15.599 | 0.011 | 38.385 | 0.033 |
| 050706_RP_FI-10 | 40 | +++ | 2.06034 | 0.00083 | 0.83701 | 0.00027 | 18.663 | 0.012 | 15.622 | 0.011 | 38.452 | 0.032 |
| 050706_RP_FI-11 | 35 | +++ | 2.05861 | 0.00080 | 0.83673 | 0.00027 | 18.635 | 0.014 | 15.593 | 0.012 | 38.362 | 0.033 |
| 050706_RP_FI-12 | 35 | ++(+) | 2.05935 | 0.00097 | 0.83697 | 0.00031 | 18.635 | 0.019 | 15.597 | 0.017 | 38.375 | 0.047 |
| **Average** | | | **2.05934** | | **0.83684** | | **18.648** | | **15.606** | | **38.402** | |
| **2 SD (abs.)** | | | **0.00124** | | **0.00031** | | **0.021** | | **0.020** | | **0.061** | |
| **2 SD (ppm)** | | | **604** | | **370** | | **1124** | | **1274** | | **1596** | |
| **2 SE (abs.)** | | | **0.00037** | | **0.00009** | | **0.006** | | **0.006** | | **0.018** | |
| **2 SE (ppm)** | | | **182** | | **112** | | **339** | | **384** | | **481** | |
| Bulk signal integration; wide interval | | | | | | | | | | | | |
| 050706_RP_FI-1 | 30 | +++ | 2.05823 | 0.00074 | 0.83652 | 0.00027 | 18.650 | 0.020 | 15.601 | 0.017 | 38.385 | 0.043 |
| 050706_RP_FI-2 | 30 | +++ | 2.05898 | 0.00080 | 0.83662 | 0.00027 | 18.651 | 0.017 | 15.604 | 0.014 | 38.401 | 0.038 |
| 050706_RP_FI-3 | 35 | +++ | 2.05881 | 0.00076 | 0.83650 | 0.00027 | 18.656 | 0.017 | 15.606 | 0.015 | 38.408 | 0.039 |
| 050706_RP_FI-4 | 40 | +++ | 2.05905 | 0.00079 | 0.83670 | 0.00027 | 18.647 | 0.015 | 15.602 | 0.013 | 38.394 | 0.035 |
| 050706_RP_FI-5 | 40 | +++ | 2.05921 | 0.00081 | 0.83696 | 0.00029 | 18.641 | 0.024 | 15.602 | 0.021 | 38.385 | 0.052 |
| 050706_RP_FI-6 | 30 | +++ | 2.06034 | 0.00079 | 0.83705 | 0.00027 | 18.660 | 0.014 | 15.619 | 0.013 | 38.444 | 0.034 |
| 050706_RP_FI-7 | 50 | ++(+) | 2.05988 | 0.00076 | 0.83695 | 0.00026 | 18.665 | 0.013 | 15.622 | 0.012 | 38.447 | 0.032 |
| *050706_RP_FI-8* | 75 | ++ | *2.05853* | *0.00064* | *0.83626* | *0.00024* | *18.669* | *0.009* | *15.612* | *0.008* | *38.429* | *0.021* |
| 050706_RP_FI-9 | 35 | +++ | 2.05992 | 0.00072 | 0.83693 | 0.00025 | 18.653 | 0.012 | 15.611 | 0.010 | 38.422 | 0.028 |
| 050706_RP_FI-10 | 40 | +++ | 2.06026 | 0.00070 | 0.83698 | 0.00025 | 18.669 | 0.012 | 15.626 | 0.010 | 38.463 | 0.027 |
| 050706_RP_FI-11 | 35 | +++ | 2.05870 | 0.00067 | 0.83671 | 0.00025 | 18.639 | 0.016 | 15.595 | 0.013 | 38.371 | 0.034 |
| 050706_RP_FI-12 | 35 | ++(+) | 2.05908 | 0.00083 | 0.83672 | 0.00029 | 18.643 | 0.019 | 15.599 | 0.017 | 38.387 | 0.044 |
| **Average** | | | **2.05931** | | **0.83679** | | **18.652** | | **15.608** | | **38.410** | |
| **2 SD (abs.)** | | | **0.00137** | | **0.00039** | | **0.020** | | **0.020** | | **0.061** | |
| **2 SD (ppm)** | | | **665** | | **464** | | **1051** | | **1302** | | **1580** | |

**Table 5** (*Contd.*)

| Sample | FI size/μm | Ablation quality[b] | $^{208}Pb/^{206}Pb$ | CI 95%[c] | $^{207}Pb/^{206}Pb$ | CI 95%[c] | $^{206}Pb/^{204}Pb$ | CI 95% [c] | $^{207}Pb/^{204}Pb$ | CI 95%[c] | $^{208}Pb/^{204}Pb$ | CI 95%[c] |
|---|---|---|---|---|---|---|---|---|---|---|---|---|
| **2 SE (abs.)** | | | **0.00041** | | **0.00012** | | **0.006** | | **0.006** | | **0.018** | |
| **2 SE (ppm)** | | | **201** | | **140** | | **317** | | **392** | | **476** | |

[a] Values in italics were excluded from calculation of averages because fluid inclusion ablation was not well controlled. [b] Quality of fluid inclusion ablation as visually judged on monitor screen (+++ = excellent; ++ = acceptable; + = poor). [c] Refers to absolute uncertainties expressed as the 95% confidence limit calculated following Baxter *et al.*[26]

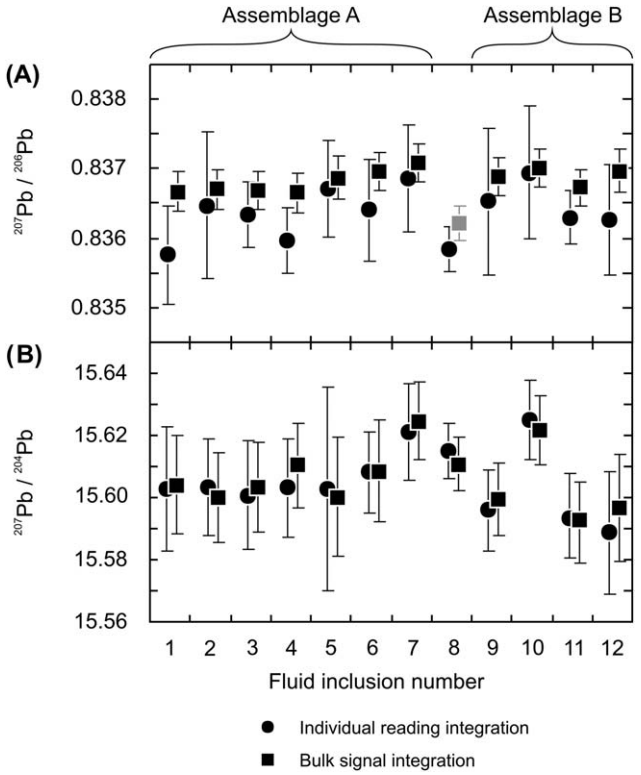


**Fig. 8** $^{207}Pb/^{206}Pb$ (A) and $^{207}Pb/^{204}Pb$ (B) isotope ratios determined for 12 fluid inclusions of *ca.* 40 × 30 × 30 μm size from a natural vein quartz sample analyzed with desolvated Tl aerosol admixed for mass bias correction. Inclusions from assemblages (A) and (B) show indistinguishable Pb isotopic compositions. The grey data point identifies an outlier. Error bars are 2 SE measurement uncertainties.

±0.032% (2 SD) for Pb isotope ratios measured relative to mass 204, or 0.0026 and 0.0075% 2 SE ($n = 18$), respectively, significantly more precise than LA-ICP-MS results obtained on single collector instruments as reported in the literature. The challenge of analyzing an individual fluid inclusion lies in the fact that it contains a strictly limited mass of analyte, of the order of 0.1 ng of Pb for inclusions of 40 × 40 × 30 μm in size, to be measured during a short time interval. External reproducibilities obtained on natural fluid inclusion assemblages were as good as *ca.* 0.05% 2 SD ($n = 11$) for $^{208}Pb/^{206}Pb$ and $^{207}Pb/^{206}Pb$, and *ca.* 0.13% for Pb isotope ratios normalized to mass 204. Acceptably reproducible results (±0.1% and 0.5%, respectively) were obtained for inclusions containing as little as 0.005 ng Pb with the current procedure.

Our study shows that a standard LA-MC-ICP-MS instrument equipped with Faraday detectors such as Nu Plasma or Nu Plasma 1700 can successfully be employed for Pb isotope analysis of individual fluid inclusions. MC-ICP-MS instruments equipped with multiple ion counters can significantly reduce the amount of Pb required for analysis, but accuracy has been shown to be somewhat limited (to *ca.* ±0.1% uncertainty) due to ion counter gain stability issues.[13,45,46] This is about an order of magnitude higher than the analytical precision obtained here for $^{208}Pb/^{206}Pb$ and $^{207}Pb/^{206}Pb$ ratios on SRM 610 glass. Ion counting, however, would be of advantage for the analysis of low-Pb samples provided that careful data acquisition schemes (*e.g.*,

Cottle *et al.*[19]) are combined with the rigorous signal integration procedure introduced here.

## Acknowledgements

TP and CAH acknowledge financial support from the Swiss National Science Foundation (grants Nr. PP002-106569 and 200020-107955). We also would like to thank E. Rosu for field assistance in Romania, and the technical staff at IGP, ETH Zurich, for their continued excellent support for analytical instrumentation. Heinrich Baur and Donat Niederer have been particularly helpful in the investigation of Faraday amplifier technical issues. We thank the 2 reviewers for pointing out the issues that needed clarification.

## References

1 P. Sylvester, *Short Course Ser.–Mineral. Assoc. Can.*, 2008, **40**, 348.
2 D. Günther, A. Audétat, R. Frischknecht and C. A. Heinrich, *J. Anal. At. Spectrom.*, 1998, **13**(4), 263–270.
3 A. Audétat, D. Günther and C. A. Heinrich, *Science*, 1998, **279**, 2091–2094.
4 W. E. Halter, T. Pettke, C. A. Heinrich and B. Rothen-Rutishauser, *Chem. Geol.*, 2002, **183**, 63–86.
5 C. A. Heinrich, T. Pettke, W. E. Halter, M. Aigner-Torres, A. Audétat, D. Günther, B. Hattendorf, D. Bleiner, M. Guillong and I. Horn, *Geochim. Cosmochim. Acta*, 2003, **67**, 3473–3497.
6 T. Pettke, W. E. Halter, J. D. Webster, M. Aigner-Torres and C. A. Heinrich, *Lithos*, 2004, **78**, 333–361.
7 M. M. Allan, B. W. D. Yardley, L. J. Forbes, K. I. Shmulovich, D. A. Banks and T. J. Shepherd, *Am. Mineral.*, 2005, **90**, 1767–1775.
8 C. Spandler, J. Mavrogenes and J. Hermann, *Chem. Geol.*, 2007, **239**, 228–249.
9 T. Pettke, *Short Course Ser.–Mineral. Assoc. Can.*, 2008, **40**, 189–218.
10 A. J. Walder, I. D. Abell, I. Platzner and P. A. Freedman, *Spectrochim. Acta, Part B*, 1993, **48**, 397–402.
11 T. Hirata, *J. Anal. At. Spectrom.*, 2002, **17**, 204–210.
12 T. Hirata, Y. Hayano and T. Ohno, *J. Anal. At. Spectrom.*, 2003, **18**, 1283–1288.
13 B. Paul, J. D. Woodhead and J. Hergt, *J. Anal. At. Spectrom.*, 2005, **20**(12), 1350–1357.
14 J. Kosler, R. B. Pedersen, C. Kruber and P. J. Sylvester, *J. Anal. At. Spectrom.*, 2005, **20**, 192–199.
15 M. G. Jackson and S. R. Hart, *Earth Planet. Sci. Lett.*, 2006, **245**, 260–277.
16 C. Paton, J. D. Woodhead, J. M. Hergt, D. Phillips and S. Shee, *Geostand. Geoanal. Res.*, 2007, **31**, 321–330.
17 M. Gounelle, E. D. Young, A. Shahar, E. Tonui and A. Kearsley, *Earth Planet. Sci. Lett.*, 2007, **256**, 521–533.
18 J. Fietzke, V. Liebetrau, D. Günther, K. Gürs, K. Hametner, K. Zumholz, T. H. Hansteen and A. Eisenhauer, *J. Anal. At. Spectrom.*, 2008, **23**, 955–961.
19 J. M. Cottle, M. S. A. Horstwood and R. R. Parrish, *J. Anal. At. Spectrom.*, 2009, **24**, 1355–1363.
20 J. Woodhead, J. Hergt, S. Meffre, R. R. Large, L. Danyushevsky and S. Gilbert, *Chem. Geol.*, 2009, **262**, 344–354.
21 T. Pettke, F. Oberli and C. A. Heinrich, *Earth Planet. Sci. Lett.*, 2010, **296**, 267–277.
22 M. Rehkämper and K. Mezger, *J. Anal. At. Spectrom.*, 2000, **15**, 1451–1460.
23 J. Woodhead, *J. Anal. At. Spectrom.*, 2002, **17**, 1381–1385.
24 M. F. Thirlwall, *Chem. Geol.*, 2002, **184**, 255–279.
25 F. Albarède, P. Telouk, J. Blichert-Toft, M. Boyet, A. Agranier and B. Nelson, *Geochim. Cosmochim. Acta*, 2004, **68**, 2725–2744.
26 D. C. Baxter, I. Rodushkin, E. Engstrom and D. Malinovsky, *J. Anal. At. Spectrom.*, 2006, **21**, 427–430.
27 S. E. Jackson and D. Günther, *J. Anal. At. Spectrom.*, 2003, **18**, 205–212.
28 B. Kuhn, K. Birbaum, Y. Luo and D. Günther, *J. Anal. At. Spectrom.*, 2010, **25**, 21–27.
29 A. N. Halliday, D. C. Lee, J. N. Christensen, M. Rehkämper, W. Yi, X. Z. Luo, C. M. Hall, C. J. Ballentine, T. Pettke and C. Stirling, *Geochim. Cosmochim. Acta*, 1998, **62**, 919–940.
30 H. P. Longerich, B. J. Fryer and D. F. Strong, *Spectrochim. Acta, Part B*, 1987, **42**, 39–48.
31 J. Baker, D. Peate, T. Waight and C. Meyzen, *Chem. Geol.*, 2004, **211**, 275–303.
32 A. Audétat, D. Günther and C. A. Heinrich, *Econ. Geol.*, 2000b, **95**, 1563–1581.
33 T. Pettke, U. H. Wiechert, A. Audétat, D. Günther and C. A. Heinrich, *Geochim. Cosmochim. Acta*, 2003, **67**, A378.
34 T. Pettke, C. A. Heinrich, A. C. Ciocan and D. Günther, *J. Anal. At. Spectrom.*, 2000, **15**, 1149–1155.
35 G. D. Kamenov, P. A. Mueller and M. R. Perfit, *J. Anal. At. Spectrom.*, 2004, **19**, 1262–1267.
36 L. P. Dunstan, J. W. Gramlich, I. L. Barnes and W. C. Purdy, *J. Res. Natl. Bur. Stand. (U. S.)*, 1980, **85**, 1–10.
37 S. M. Eggins and J. M. G. Shelley, *Geostand. Newsl.*, 2002, **26**(3), 269–286.
38 A. J. R. Kent, *Geostand. Geoanal. Res.*, 2008a, **32**, 129–147.
39 B. J. A. Willigers, J. A. Baker, E. J. Krogstad and D. W. Peate, *Geochim. Cosmochim. Acta*, 2002, **66**, 1051–1066.
40 R. D. Evans, H. Hintelmann and P. J. Dillon, *J. Anal. At. Spectrom.*, 2001, **16**, 1064–1069.
41 S. Wehmeier, R. Ellam and J. Feldmann, *J. Anal. At. Spectrom.*, 2003, **18**, 1001–1007.
42 E. A. Krupp and O. F. X. Donard, *Int. J. Mass Spectrom.*, 2005, **242**, 233–242.
43 I. Günther-Leopold, J. Kobler Waldis, B. Wernli and Z. Kopajtic, *Int. J. Mass Spectrom.*, 2005, **242**, 197–202.
44 A. Audétat, D. Günther and C. A. Heinrich, *Geochim. Cosmochim. Acta*, 2000a, **64**, 3373–3393.
45 A. K. Souders and P. J. Sylvester, *J. Anal. At. Spectrom.*, 2008, **23**, 535–543.
46 A. J. R. Kent, *J. Anal. At. Spectrom.*, 2008, **23**, 968–975.

 